Numerical study of regular and irregular wave interaction with vertical breakwaters

Master of Science thesis

For obtaining the degree of Master of Science in Civil Engineering at Delft University of Technology

Mohamed Al Saady

Delft University of Technology
Department of
Civil Engineering and Geosciences

In cooperation with

Royal HaskoningDHV
Department of
Hydraulics and Morphology

Graduation committee

Prof.dr.ir. W.S.J Uijttewaal	Delft University of Technology Section of environmental fluid mechanics
Dr.ir. M. Zijlema	Delft University of Technology Section of environmental fluid mechanics
Ir. H.J. Verhagen	Delft University of Technology Section of coastal engineering
Ir. O. Nieuwenhuis	Royal HaskoningDHV Section of Hydraulics and Morphology
Ir. O. Scholl	Royal HaskoningDHV Section of Hydraulics and Morphology

Abstract

In this study regular and irregular waves are simulated with a numerical model. The aim of this study is to perform a numerical investigation into the reflection and transmission of the different waves forcing in a porous breakwaters.

There are different types of numerical models available for solving the behaviour of waves in coastal regions and harbours. The most known numerical models are Boussinesq type wave models and non-hydrostatic wave models. In this study, the non-hydrostatic approach is chosen. Last years developments shows that this approach is competitive to Boussinesq type wave models in terms of robustness and the computational resource required to attain reliable outcomes in challenging wave and flow conditions. The simulations are performed with the non-hydrostatic model called SWASH, because it is a model that still is in development a validation of the model with this study is beneficial for the development.

The influence of wave conditions and breakwater characterises on the reflection and transmissions are examined. In a number of cases the influence of the porosity, wave height, wave period and the width of the breakwater on reflection are investigated. The model predictions are found to be consistent with lab experiment, analytical solutions and empirical formulations.

The reflection and transmission of bound long waves were also studied. The influence of the relative depth (*kh*) on the reflection and transmission was investigated. The model predications on the reflection of the bound long waves are found to be consistent with lab experiment. The model prediction deviates not more than 15 percent of the experimental results. On the other hand, the transmission of short waves and bound long waves were inconsistent with lab experiment. The most likely explanation for this inconsistency is the large deviation between the breakwater geometry used in SWASH and the experiment. In SWASH it is not possible to vary the porosity in vertical direction, so it was necessary to schematize the breakwater since the used breakwater in the experiment composed of two different porosities.

A signal decomposition technique was used to quantify the magnitude of the incoming and reflected monochromatic and bi-chromatic waves. The results of the collocated method show that SWASH correctly simulates the propagation of the incoming and reflected waves.

To differentiate between the free and bound components after the waves reflect or transmit through the breakwater, the method used by Rijnsdorp et al (2014) here was also applied. This analysis is based on the difference in wave length between the bound and free component. The method produced accurate results, because before the wave reach the breakwater the wave field contains only bound waves and after reflection both free and bound waves were available in the computational domain.

Preface

This thesis is submitted in order to obtain the degree of Master in Science in Civil Engineering at the Delft University of Technology. The work was carried out in close cooperation with the Hydraulic and Morphology Engineering department of Royal HaskoningDHV.

Acknowledgments

I would like to thank all the members of my graduation committee for their great support and comments during this research. Their experience and knowledge has been very helpful to me and increased my enthusiasm for the subject. I would like to thank Prof.dr.ir Wim Uijtwaal for his guidance and feedback during this research, ir Henk jan Verhagen for this clever and useful comments on my work and dr.ir Marcel Zijlema/ ir. Dirk Rijnsdorp for helping me to overcome several challenges which I encountered with the numerical model and for the interesting conversations about wave modelling.

In addition to this I would like to thank Royal HaskoningDHV for giving me the opportunity to perform my M.Sc. thesis within their company and to cooperate with highly skilled engineers.

Finally, I want to thank my family and friends for their interest and support during my studies in Delft.

Mohamed Al Saady
Delft, July 2014

Contents

List of figures

List of Tables

1. Introduction

1.1. Background

Breakwaters are used to protect coasts and harbours from attacks of the ocean waves. An accurate prediction of the behaviour of waves approaching a porous breakwater is inevitable to forecast the sheltering capacity by the breakwaters. Reflection and transmission coefficients are the most important parameters for designing a porous breakwater and are necessarily to be accurate for various wave forcing and conditions. The different wave forcing are regular and irregular waves, most studies to determine the reflection and transmission coefficient are based on regular waves. There is very little known about the reflection and transmission of infragravity (IG) waves which are induced by irregular wave field. However, there are some studies which show the importance of IG-waves in harbours, these waves could affect harbour operations and cause large damage in harbours. Some examples of these studies are: IG-wave are found to be significant in harbour oscillations (Bowers 1977). Naciri et al. (2004) showed the importance of incorporating IG-waves in the calculation of moored vessel motions. Furthermore IG-waves may excite harbour seiches by edge waves, for example, Chen et al.(2004). Subsequently, these seiches can have a big impact on moored vessels motions (Van Der Molen et al., 2006).

Theoretical solutions for reflection and transmission of regular waves have been derived by several authors using different methods of approach. Madsen and White (1977) have developed a method for the determination of reflection and transmission coefficients of multi-layered, porous rubble-mound breakwater of trapezoidal cross-section. Further, Madsen (1983) has derived an analytical solution for the reflection of monochromatic waves from a vertical homogenous breakwater on a horizontal bottom. The reflection coefficient was determined as a function of parameters describing the incoming waves and the breakwater characteristics.

The above mentioned studies have been concerned only with monochromatic waves. The importance of reflection and transmission of IG-waves was the first time shown by Hossain et al. (2001). They obtained an analytical and experimental result for the reflection and transmission of IG-waves induced by the short-wave groups due a composite vertical breakwater.

Besides those theoretical studies empirical formulations has been performed by several researchers. Miche (1951) empirically determined the reflection coefficient for monochromatic waves breaking on a plan beach. Battjes (1974) redefined Miches hypothesis in terms of the Iribarren number or breaker parameter. Ursell et al. (1960) and Seeling and Ahrens (1981) indicated that Miches equation significantly overestimated the reflection of both regular and irregular waves and presented an improved estimation of the reflection coefficient.

In the last decades researchers have developed numerous phase resolving numerical models. These phase resolving models could be used to predict generation, propagation, reflection and transmission of waves. Delft University of Technology has developed a non-hydrostatic model called SWASH (Simulating Waves till SHore). The model is intended to be used for predicting transformation of surface waves and rapidly varying shallow water flows in coastal waters. In this study the non-hydrostatic model SWASH will be used to investigate the reflection and transmission of different

waves forcing and different type of porous structures. As this model has never been tested for reflection and transmission of irregular (bi-chromatic) waves.

1.2. Objectives

This study will focus on reflection and transmission of regular and irregular waves through porous structures. The capability of the numerical model SWASH will be tested in simulations the reflection and transmission of different wave forcing and type of structures. So far, SWASH has only been validated for the transmission and reflection of regular waves.

The main objectives of this thesis:

- To determine the influence of different physical parameter (e.g. porosity, wave height and wave period) on the reflection coefficient. And indicate the capability of SWASH in predicting reflection coefficient for regular wave forcing.

- Establish the capability of SWASH in predicting reflection and transmission of breakwater for irregular (bi-chromatic) waves.

1.3. Approach

The next steps will be followed to realise the objective mentioned in the previous section.

SWASH will be used to produce analytical solutions concerning the reflection through porous structures performed by Madsen (1983). Further SWASH results will be compared with empirical solutions performed by Seelig (1980).

SWASH will be used to produce experimental results performed by Hossain et al (2001). They obtained experimental results for the reflection and transmission IG-waves due a composite vertical breakwater.

1.4. Guide line

The remainder of this master thesis is organized as follows:

Chapter 2 focuses on the theoretical basis needed throughout this thesis, e.g. theory on regular and irregular waves and porous flows. A detailed description of the model SWASH is given in Chapter 3 in order to assess the capabilities and limitations of the numerical model. In chapter 4 the results of SWASH will be extensively analysed to investigate whether the model is capable of correctly simulating reflection by monochromatic waves. The influence on reflection for different physical parameters is analysed. Further, the reflection and transmission of bi-chromatic waves is also investigated. In chapter 5 the results are summarised and some recommendations for further studies are presented.

2. Physics of waves and porous structures

This chapter describes the literature relevant for this study. The reflection and transmission of waves through porous structures depend on the wave forcing (regular or irregular) and breakwater characteristics. That is why a short description of waves will be given, firstly. Secondly, analytical solution and empirical formulation for porous structures used in this study will be discussed. Finally, relevant performed experiments which can be used for this study are summarized.

2.1. Waves

Various types of waves can be distinguished in oceans and coastal waters. Sorting the various waves by their frequencies gives an overview of the various wave types that can be encountered in oceanic and coastal water Figure 1. The wave period can vary from seconds (capillary waves) up to 24 hours (trans-tidal waves). In this study the focus is on behaviour of monochromatic and bi-chromatic waves with a period range from 1 till 100 sec.

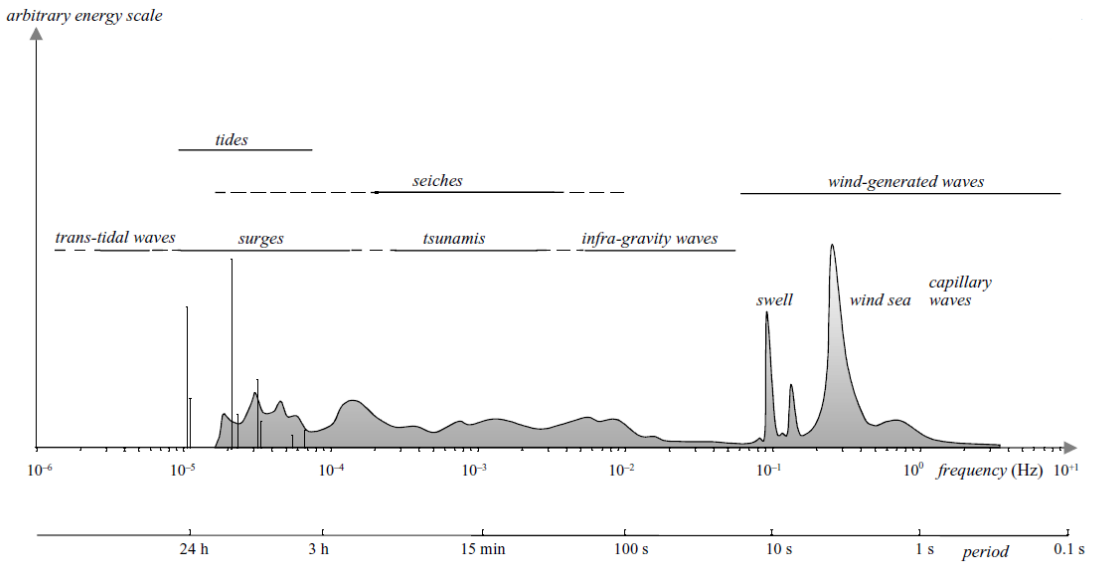

Figure 1: Frequencies and periods of the vertical motions encountered at the ocean surface, after Holthuijsen (2007).

Ocean waves can be described by linear wave theory. The most interesting result of this theory is a long-crested propagating harmonic wave. Based on this theory, many wave characteristics can be derived. Besides this, most theories on wave transmission are based on linear wave theory. In order to understand the behaviour of waves and its characteristics, an explanation of linear wave theory is given. For more detailed information and the derivations of the formulas given below, one is referenced to Holthuijsen (2007) and Appendix A.

2.1.1. Regular waves

The most interesting result of linear wave theory is a long-crested propagating harmonic wave. This harmonic wave (regular wave) can be defined as propagating sinusoidal wave with an amplitude (*a*), radian frequency (*ω*) and wave number (*k*). The equation of the sinusoidal harmonic wave is shown below.

$$\eta(x,t) = \frac{1}{2} H \sin\left(\frac{2\pi}{T} - \frac{2\pi x}{L} \right) = a \sin\left(\omega t - kx \right)$$

The phase speed is the forward speed (*c*) by which the wave propagates while the phase (*ωt-kx*) remains constant. Mathematically this implies that the time derivative of the phase is zero. From this the phase speed is obtained equation. The parameters used in the equation are shown in Figure 2.

$$c = \frac{\omega}{k} = \frac{L}{T}$$

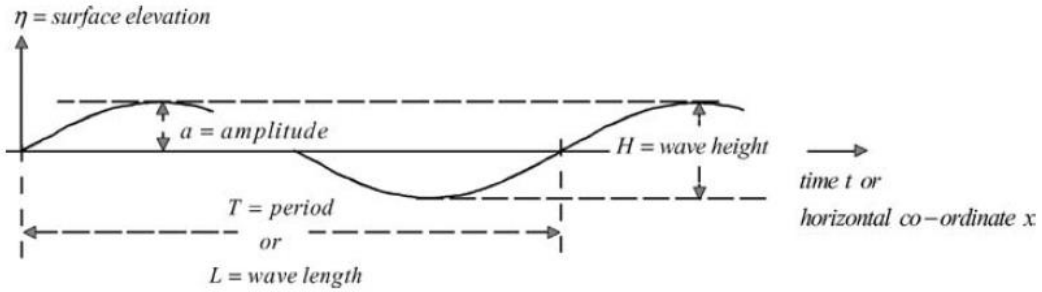

Figure 2: Propagating harmonic sine wave, (Holthuijsen, 2007).

2.1.2. Irregular waves

If one observes the water surface, it can be seen that it continuously changes without repeating itself. When the water surface elevation is measured, the resulting signal will be like an irregular wave signal, which can be modelled by the sum of a large number of harmonic wave components:

$$\eta(t) = \sum_{i=1}^{N} a_i \cos\left(2\pi f_i t + \alpha_i \right)$$

In which, *N* =large number of frequencies, a_i =amplitude, α_i =phase, f_i = wave frequency

Each wave component is propagating as regular wave which has a sinusoidal shape. From this it follows that the irregular wave signal, which describes the surface elevation, can be decomposed by a Fourier series into a number of harmonic waves, see Figure 3. The results are a set of values for the amplitude (*a*) and phase (*α*). Each set of values of *a* and *α* belongs to the frequency *f*. The benefit of this concept is that it is possible to describe the waves as a spectrum. Waves are propagating in a certain direction. The direction can be taken into account by considering positive *x*-axis and using the principles for the one-dimensional variance density spectrum.

From the variance density spectrum it is relatively easy to obtain a wave energy density spectrum. This can be obtained by multiplying the variance density spectrum with the density of the water and with the gravitational acceleration.

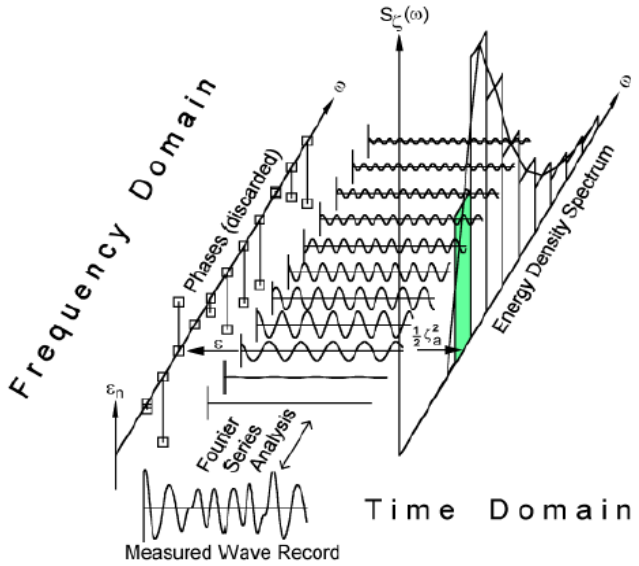

Figure 3: Wave record analyses, ζ_a represent wave amplitude, (Journee and massi, 2001)

2.1.2.1. Infragravity waves

The simplest form of irregular waves is the bi-chromatic waves. Figure 4 shows a bi-chromatic wave signal, which is a superposition of two sinusoidal wave signals. The modulation of the short wave height on wave group scale results in a gradient in the radiation stress on similar scale. This radiation stress gradient is balanced by a force that expels the fluid under regions of this wave, creating a local depression. The resulting pattern of the surface elevation is in anti-phase with and phase locked to the wave groups (the pattern travels with the group velocity). This pattern is recognized as an IG-wave bound to the wave groups and referred to as a bound IG-wave.

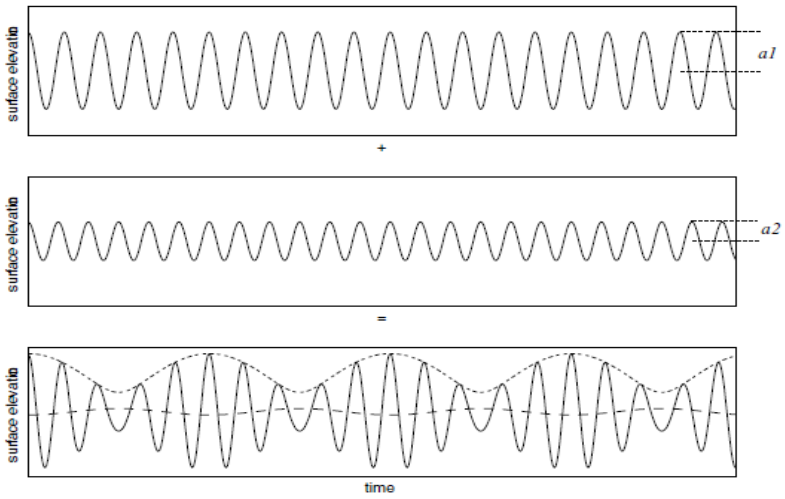

Figure 4: Upper two panels show the primary waves (solid lines), the lowest panel shows the superposition of the two primary waves and the amplitude envelope. The dash-dot line represents the bound long wave.

In the literature two generation mechanisms of free IG-waves are recognized. The first mechanism is the release of bound IG-waves in the surf zone. As the short waves propagate in shoreward direction, they start to break in the surfzone. IG-waves will not fully dissipate as they reach the shoreline and get reflected at the shoreline.

Another generation mechanism of free IG-waves is presented by Symonds et al. (1982), who treated the variation of the breakpoint location in time due to the group structure of the incident waves. As the waves break, a strong gradient in the radiation stress develops due to the dissipation of wave energy. This radiation stress gradient results in a set up at the shoreline, whereby higher waves results in greater setup than relative low waves. Due to the group structure of the incident waves and the resulting time-varying breakpoint, the resulting set up is not constant but varies on the wave group time scale. This time varying setup is considered as a shoreward propagating free IG-waves, which is in phase with the wave groups.

2.2. Porous flows

Previous researchers have experimentally and analytically studied wave reflection for a variety of structures. A short overview of performed experiments and theories is given below.

Various prediction techniques have been proposed to estimate reflection coefficients for specific types of energy dissipation. Miche (1951) proposed a wave reflection coefficient prediction technique that often mentioned in literature. He assumed that there is some critical deep water wave steepness below which the reflection coefficient is constant. For conditions where wave steepness is greater than the critical value, the reflection coefficient is proportional to the ratio of the wave steepness to critical value of wave steepness. Predictions using Miches approach give the right order of magnitude estimate of the reflection coefficient, but as Ursell et al (1960) illustrated, predictions may be conservative by a factor of 2.

Moraes (1970) has performed some of the most extensive laboratory test on monochromatic wave reflection from a variety of smooth and rough slopes.

Madsen and White (1976) made a number of additional carefully controlled reflection measurements for smooth and rough steep sloped structures under nonbreaking wave action. Based on these data, they developed an analytical empirical model for predicting reflection coefficients for rough slopes with nonbreaking waves. Further, Madsen (1983) has derived an analytical solution for the reflection of monochromatic waves from a vertical homogenous wave absorber on a horizontal bottom. He expressed the reflection coefficient as a function of several physical parameters.

Battjes (1974) used Moraes data to develop an equation for predicting reflection coefficients for smooth slopes where the slope induces wave breaking. This technique is conservative for nonbreaking waves. Ahrens (1980) has made a number of irregular wave reflection coefficient measurements for overtopped and non-overtopped plan smooth slopes.

A number of wave reflection measurements for laboratory breakwater have been made. Seelig (1980) investigated rubble-mound and caisson breakwaters using regular and irregular waves. Gunbak and Brunn (1979) measured reflection coefficients for rubble-mound breakwaters and proposed and empirical prediction technique. A comparison of wave reflection coefficient for various equations is given in Figure 5.

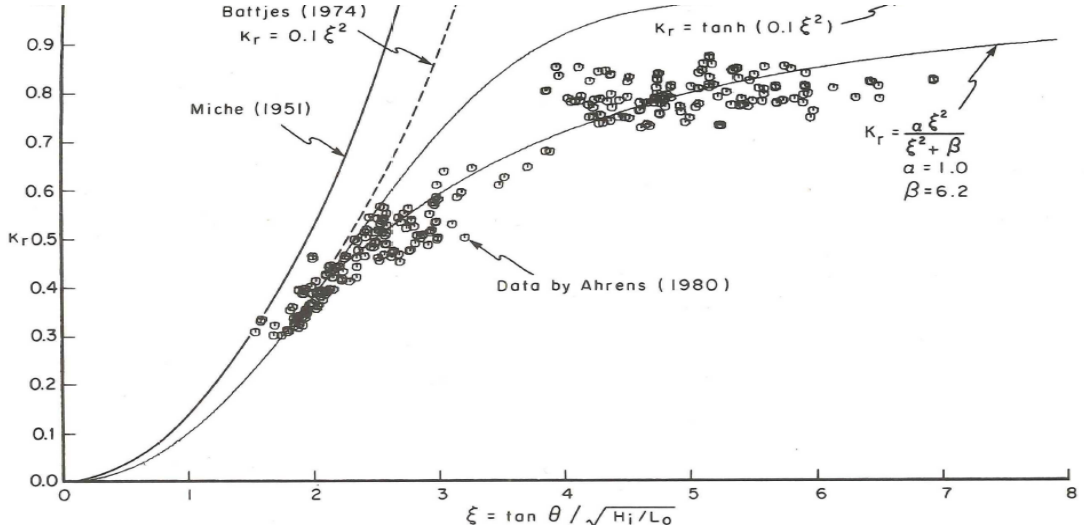

Figure 5 : A comparison of wave reflection equations to predicted reflection coefficient, from report: Seelig, W. N., & Ahrens, J. P. (1981); here, ξ= Iribarren number, k_r= reflection coefficient.

In the next sections a closer view is made to theories and experiments which will be used in chapter 4 to compare the SWASH results.

2.2.1. Analytical solution Madsen

As mentioned in the introduction Madsen (1983) has derived an analytical solution to determine the reflection coefficient as function of several physical parameters. This has been done for a vertical rubble mound breakwater in the front of closed wall. The case studied by Madsen is shown in Figure 6.

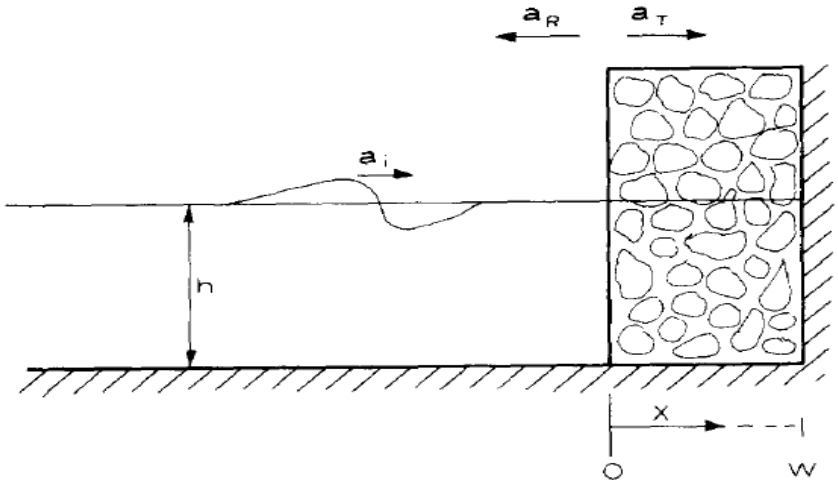

Figure 6: definition sketch, by Madsen 1983.

For the porous part the governing equation for the motion are:

$$n\frac{\partial \xi}{\partial t} + h\frac{\partial u}{\partial x} = 0$$

$$\frac{1}{n}\frac{\partial u}{\partial t} + g\frac{\partial \xi}{\partial x} + U(\alpha + \beta|U|) = 0$$

Where α and β account for the laminar and turbulent friction loss respectively and *n* is the porosity of the structure.

The non-linear friction term is linearized by using the approximation

$$U(\alpha + \beta|U|) = f\frac{\omega}{n}U$$

Where *f* is the friction factor which will be assumed to be independent of *x* and *t*. Because of the linearized equations it is possible to look for a periodic solution with radian frequency *ω*, the system can be solved taking:

$$\xi = \mathrm{Re}\left[\eta(x)\,\mathrm{e}^{i\omega t}\right]$$

$$U = \mathrm{Re}\left[\upsilon(x)\,\mathrm{e}^{i\omega t}\right]$$

Eventually after applying algebraic manipulations described in (Madsen 1983), it is possible to derive and analytical expressions for the complex amplitude of the reflected wave:

$$\frac{a_r}{a_i} = \frac{1-\varepsilon+(1+\varepsilon)e^{-i2\kappa w}}{1+\varepsilon+(1-\varepsilon)e^{-i2\kappa w}}$$

In which,

$$\varepsilon = \frac{n}{\sqrt{1-if}} \qquad \kappa = \frac{\omega}{\sqrt{gh}}\sqrt{1-if}$$

The reflection coefficient can be determined from equation as function of

1. Porosity (*n*)
2. Width of breakwater (*w*)
3. Incoming wave amplitude (a_i)
4. The diameter of the stones/grains (*d*)
5. The water depth (*h*)
6. The wave period (*T*)

2.2.1.1. Determination of the friction factor

The reflection coefficient has been derived as function of the friction factor (*f)*, the porosity (*n)* and of the wavenumber multiplied by the width of the breakwater (*kw*). However, in order to make a predictive solution, the friction factor (*f*) must be related to parameters describing the incoming waves as well as the breakwater characteristics. To do this the Lorentz principle of equivalent work is applied. This principle states that the average rate of energy dissipation should be identical whether using the true non-linear resistance law or its linearized equivalent:

$$\int_0^W \int_0^T f \frac{\omega}{n} U^2 dt dx = \int_0^W \int_0^T \left(\alpha + \beta |U|\right) U^2 dt dx$$

In which *T* is the wave period and *w* the width of the breakwater. The value of *U* should be corresponds to the general solution for the flow inside the breakwater.

$$U = a_i \sqrt{\frac{g}{h}} \mathrm{Re}\left\{ \frac{2\varepsilon(\mathrm{e}^{-\mathrm{i}kx} - \mathrm{e}^{\mathrm{i}\kappa(x-2w)})}{1+\varepsilon+(1-\varepsilon)\mathrm{e}^{-i2\kappa w}} \mathrm{e}^{\mathrm{i}\omega t} \right\}, \quad 0 \le x \le w$$

Substituting U into the linearized Lorentz and rearranging terms finally leads to an equation which can be used for the determination of friction coefficient (*f).*

$$F = 0$$

In which:

$$F \equiv \alpha_0 \frac{(1-n)^3}{n} \left(\frac{\upsilon T}{2\pi d^2} \right) + \beta_0 \frac{(1-n)}{n^2} \frac{a_i}{2\pi d} T \sqrt{\frac{g}{h}} \Lambda - f$$

$$\Lambda \equiv \frac{\int_0^W \int_0^T |U^*| U^{*2} dt dx}{\int_0^W \int_0^T U^{*2} dt dx}$$

$$U^* = \mathrm{Re}\left\{ \frac{2\varepsilon\left(\mathrm{e}^{-\kappa x} - \mathrm{e}^{\mathrm{i}k(x-2w)}\right)}{1+\varepsilon+(1-\varepsilon)\mathrm{e}^{-i2\kappa w}} \mathrm{e}^{\mathrm{i}wt} \right\}$$

The friction coefficient has to be solved by numerical iteration. An outline of the procedure is given below:

1. Assume two initial values for *f,* say *f* = 0 and f =1.
2. Compute *ε*, *κ* and *U** for these two values.
3. Compute Λ by integration and determine *F* for these two values of *f.*
4. Determine a new value of *f* by using the method:

$$f_{n+1} = \frac{F(f_n) f_{n-1} - F(f_{n-1}) f_n}{F(f_n) - F(f_{n-1})}$$

2.2.2. Empirical formulation Seelig

Seelig (1980) did use an experimental data set to derive an empirical relation for the reflection. The derived formulation reads as follow

$$k_r = \frac{a * \xi^2}{\xi^2 + b}$$

In which: k_r = reflection coefficient; *a* and *b* = empirical coefficients; ξ = irribaren number

The values of coefficients *a* and *b* depend primarily on the structure geometry and to a smaller extent on whether waves are monochromatic or irregular. The irribaren number employs the structure slope and the wave height at the toe of the structure.

The source of data and ranges of condition where the method could be applied is given in Table 1.

Table 1: source of data and range of conditions, from report: Seelig, W. N., & Ahrens, J. P. (1981)

Data set	Reference	Struc types[1]	Cotθ of structure seaward slopes	Wave types[2]	$\frac{d_s}{gT^2}$	$\frac{d}{d_s}$	$\frac{H_I}{H_b}$	$\frac{d}{L}$	n [3]	K_r, calculation method[4]
a	Ahrens (1980)	1	1.5-2.5	I	0.005-0.04	0.0	0.06-1.0	0.0	0	B
b	Ahrens and Seelig (1980)	2	2.0	S,I	0.001-0.025	0.11-0.2	0.16-1.0	0.004-0.02	2.5	B
c	Debok and Sollitt (1978)	3	1.5-2.0	S	0.031-0.14	0.12-0.17	0.28-1.0	0.010-0.024	1	A
d	Gunbak (1979)	3	1.5,2.5	S	---	0.03	---	---	--	A
e	Madsen and White (1976)	1,2	1.5-3.0	S	0.0078-0.012	0.0-0.17	0.07-0.25	0.0-0.02	1	C
f	Moraes (1970)	1,2	0-10.0	S	0.008-0.035	0.002-0.054	0.0-0.34	0.0-0.007	1	A*
g	Seelig (1980)	3	1.5-2.6	S,I	0.002-0.08	0.04-0.61	0.0-1.0	0.0-0.096	1,2	B
h	Hydraulics Research Station (1970)	4	1.5	S,I	0.0067-0.015	0.09	0.3-0.8	0.004-0.013	2	A
i	This study	1,2	2.5,15.0	S,I	0.0018-0.044	0.0-0.22	0.06-0.7	0.0-0.37	0,1,2,3,4	E
j	Ursell, Dean, and Yu (1960)	1	15.0	S	0.0014-0.13	0.0	0.05-0.44	0.0	0	A
k	Chesnutt (1978)	5	5.0-5.9	S	0.005-0.032	0.003	0.2-0.36	0.00008-0.0002	--	A

[1]Structure types:
1, smooth impermeable revetment (nonovertopped);
2, impermeable revetment with one or more layers of armor;
3, rubble-mound breakwaters (rough, permeable);
4, dolos breakwater;
5, laboratory beach.

[2]Wave types tested:
S, sine blade motion;
I, irregular waves.

[3]n = number of layers of armor

[4]Reflection coefficient calculation method:
A, envelope method;
A*, modified envelope method (Goda and Abe, 1968);
B, method of Goda and Suzuki (1976);
C, method of Madsen and White (1976).

The formulation of Seelig (1980) is applicable for rubble-mound breakwaters with one or two armour layers. The different parameters used in the table are explained below.

The water depth at the toe of the structure, *ds*, is taken as a characteristic water depth, *g* is the acceleration due to gravity, and representative armour unit diameter, *D*, is determined from

$$D = \left(\frac{w}{\gamma} \right)^{1/3}$$

In which w is the armour weight and γ the specific weight of the armour material. A measure of the breakwater height that could occur at the toe of the structure, h_b, is given by Goda (1975) as

$$h_b = 0.17 L_0 \left\{ \left(1 - \exp\left[-4.712 \frac{ds}{L_0} \left(1.0 + 15 m^{1/3} \right) \right] \right) \right\}$$

In which L_0 is the deep water length given by linear wave theory, and m is the tangent of the slope of the seabed seaward of the structure.

Other variables that are summarized in Table 1 include dimensionless ratios using H_i, the incident wave height at toe of the structure; T, the wave period and L, the wavelength at the toe of the structure.

2.3. Previous lab experiments

Two different experiments will be used to compare the SWASH model results in chapter 4. The first experiment consider regular waves and the second uses irregular (bichromatic) waves. A summary of the performed experiments is given in this section.

2.3.1. Monochromatic experiments

The experiments were carried out in the large flume of environmental fluid mechanics laboratory of the TU Delft. The length of the flume is 38 m. The testing breakwaters are placed in the flume at 28 meter form the wavemaker. A sketch of the setup is included in Figure 7.

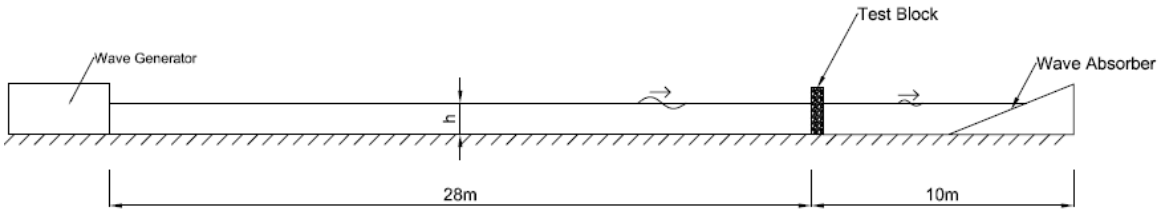

Figure 7: experimental setup, Mellink (2012)

The wavemaker is capable of creating monochromatic waves where the user should choose the period, wave height and water depth. It uses an automated reflection compensator in order to minimize wave reflections created from the wave board. As a result, it is ensured that the incoming signal is the desired wave signal at all times. Further to damp waves which are transmitted through the breakwater, a structure is placed on a 1:3 slope at the end of the flume.

Different breakwaters were used to determine the reflection and transmission. A summary of the most important information per breakwater can be found in Figure 8 .

	Material	Thickness (mm)	d_{n50} (m)	n (-)	k (m/s)	α (-)	β (-)	Re_d (-)
1	Yellow sun lime-stone 8-11 mm	39	0.007	0.386	0.065	700	1.1	220
2	Yellow sun lime-stone 20-40 mm	88	0.020	0.405	0.136	1200 (est.)	1.25 (est.)	2100
3	Yellow sun lime-stone 20-40 mm	132	0.020	0.423	0.131	1200	1.25	2700
4	Norwergian >40 mm	80	0.039	0.41	0.154	1900	1.7	6000
5	Norwergian >40 mm	160	0.039	0.466	0.214	1150	1.6	7850
6	Norwergian >40 mm	240	0.039	0.46	0.213	1020	1.45	8300

Figure 8: description of the breakwaters

The data for breakwater 5 and 6 are taken to compare with the SWASH results, since those blocks are in the range within the simulations are performed. The results for the reflection as function of the breakwater width (w) multiplied with the wave number (k) are given in Table 2.

Table 2: Reflection coefficient as function of breakwater width multiplied with wave number; Mellink (2012)

kw	reflection coefficient
0.14	0.55
0.21	0.57
0.23	0.6
0.32	0.64
0.34	0.65
0.49	0.68

2.3.2. Bichromatic experiment

Hossain et al. (2001) carried out experiments in the research flume of fluid Mechanics Laboratory of the Department of Civil Engineering at Nagoya Institute of Technology, Japan. The experiments are carried in wave flume of 26 m long, 0.6 m wide and 1.2 m height with glass wall at both sides. An irregular wave generator was used to generate the wave group and associated bound long waves. To minimize the effects of re-reflections between the breakwater and the wave generator, only first 2 to 3 group waves were used in the analysis.

A composite breakwater with parameters, *d/h*=0.6 and *b/h*=0.8 was built in the wave flume in constant water depth of *h*=0.4 m as illustrated in Figure 9. The porous part of the breakwater was filled with gravel of mean diameter 0.02 m and porosity *n* = 0.45.

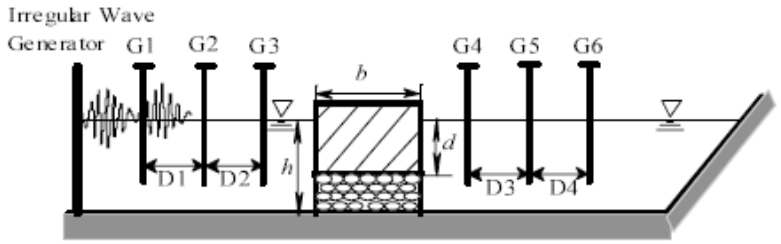

Figure 9: experimental setup

Three capacitance-type wave gauges were installed in the seaward side of the breakwater at intervals of *D1* = 2.15 m and *D2* = 2.45 m. Three wave gauges were also installed in the leeward side of the breakwater at intervals of *D3* = *D4* + 1.55 m to measure the transmitted waves. A total of ten different sets of experiments were conducted varying the central wave period from 1.1 to 2.0 s as shown in Table 3, which cover the relative depth *kh* form 0.68 to 1.47. Wave groups of two short-wave components having equal amplitude of *A1*=*A2*=0.027m were used throughout the experiments.

The time series measured by the set of three wave gauges are used to separate different long wave components in the seaward and leeward sides of the breakwater. The amplitudes of reflected/transmitted bound long wave in the seaward and leeward sides of the breakwater are very small throughout the experiments and ignored in the analysis.

The linear friction factor *f* used in the calculations depends on the Ursel number of incident waves. The friction factor *f* is determined through the iterative method using Lorentz principle of equivalent works. In the calculations, the intrinsic permeability k_p = 1.8 m^2 and the non-dimensional resistance coefficient C_f = 0.29 are given from the experimental conditions. The resultant friction factor *f* corresponding to the experimental conditions ranges from 2.5 to 3.8

The result for the transmission of short waves, transmission IG-waves and the reflection as function of *kh* are given in Table 3.

Table 3: experiment results; determined by Hossain et al. (2001)

kh	Trans. short waves	Trans. IG-waves	Refl. IG-waves
0.68	0.3	0.84	0.6
0.72	0.31	0.83	0.7
0.78	0.26	0.84	0.62
0.82	0.28	0.76	0.75
0.88	0.27	0.79	0.78
0.95	0.26	0.84	0.64
1.04	0.27	0.81	0.81
1.14	0.23	0.87	0.79
1.28	0.21	0.96	0.85
1.47	0.2	1	0.86

3. Numerical models

3.1. Introduction

There are different types of numerical models available for solving the behaviour of waves in coastal regions and harbours. The most known numerical models are Boussinesq types wave models (e.g Madsen et al., 1991) and non-hydrostatic wave models (e.g. Stelling and Zijlema, 2003). These models resolve the wave field on the timescale of individual waves and are as such capable of modelling the non-linear evolution of the wave field accurately.

Traditionally the Boussinesq models, which have been designed specifically for wave propagation, were more efficient models. Non-hydrostatic models needed a high resolution in the vertical (twenty layers) to obtain similar results to the depth averaged formulated Boussinesq models. The resulting difference in computational time resulted in a focus on the development of Boussinesq models for coastal engineering practice.

Stelling and Zijlema (2003) showed that, using an edge based finite difference scheme in the vertical, it is possible to construct a non-hydrostatic model that is competitive to the Boussinesq models. For linear wave propagation their model gives similar results to higher order Boussinesq models while with only two computational layers and for a single layer the model is comparable to low order Boussineq models.

In this chapter, a short description of both models and the main advantages/disadvantages are given below. Further, the difference in determining the reflection coefficient for two type of models (SWASH; Non-hydrostatic approach and Mike21; Boussinesq) are highlighted.

3.2. Description of Boussinesq and non-hydrostatic approaches

3.2.1. Boussinesq-type

The Boussinesq-type wave models have rapidly gained large popularity; since researchers have concluded that the model is capable in reproducing laboratory data and field measurements for coastal regions and harbours.

The corresponding equations are vertically integrated equations for wave propagation in two horizontal dimensions with different assumptions made for the variation of fluid motion over the water depth. As such, they can be interpreted as extended shallow water equations including the lowest order effects of frequency dispersion and nonlinearity. In addition, they can resolve rapid variation that occur at scales of one wave length or lesser.

Most well-known and well established Boussinesq-type wave models are FUNWAVE (Kirby et al., 1998), BOUSS-2D (NWOGU and Demirbilek, 2001) and Mike 21 BW (DHI Group, 2008). Numerous researchers and users all over the world contributed to the testing, development and refinement.

General principles of Boussinesq type wave models

- Boussinesq-type wave models are phase resolving, they describe individual wave behaviour.
- Within the Boussinesq-type wave model the 3D flow is written in 2D equations.
- The Boussinesq-type wave models are capable of reproducing the most important wave phenomena like: shoaling, refraction, diffraction, wave breaking, bottom dissipation, moving shoreline (run-up and run-down), partial reflection, wave transmission, non-linear wave-wave interactions, frequency spreading and directional spreading.

Short coming Boussinsq models

Physical effects as, wave breaking and moving shoreline in Boussinesq model gives large problems for the modellers. Yet the modelling of those physical process still poses difficulties because of the an apparent need to employ empirical formulations and numerical schemes of much greater complexity than had been used so far to model other wave processes such as dispersion, shoaling, refraction and diffraction. These difficulties include uncertainly on choice of empirical parameters, complexity of implementation, reduced numerical stability and robustness, high computational costs and the need for greater physical accuracy.

3.2.2. Non-hydrostatic models

An alternative approach to model waves is the non-hydrostatic approach. The nonlinear shallow water equations (NLSW) are mathematically equivalent to the Euler equation for compressible flows. Discontinues are admitted through the weak form of these equations and can take the form of bores which are hydraulic equivalent of shock waves in aerodynamics. The conservation of energy does not hold across the discontinuities but the conservation of mass and momentum remains valid. By considering the similarity between broken wave and steady bores, energy dissipation due to turbulence generated by wave breaking is inherently accounted for. In the pre-breaking region, however, the NLSW equations do not hold as they assume a hydrostatic pressure distribution, and thus prohibit a correct modelling of dispersive waves. However by extending the NLWS equations to include the effect of vertical acceleration, the propagation of those waves can be simulated.

Over the past few years, Delft University of Technology has made a strong effort to develop a wave model for simulations in coastal regions. Below is a description given of the model that has been developed.

SWASH (Simulating Waves till Shore) is a hydrodynamic model for simulating non-hydrostatic, rational free-surface flows. The model is based on the nonlinear shallow water equations including the non-hydrostatic pressure. Several papers provide a more detailed description of the model equations and the numerical implementation (Stelling and Zijlema, 2003), (Zijlema and Stelling 2005) and Zijlema et al. (2011). These phase-resolving models account for all relevant near-shore processes (e.g. shoaling, refraction, reflection and non-linearity) and thereby provide a more accurate, but computationally more expensive approach.

Recently, the model got extended into covering porous flow and the ability to predict partial reflection and transmission. The Forchheimer relation is included in the porous momentum equation by means of two extra friction terms f_l and f_t . Every grid cell has a porosity ranging from n=0 (wall) till n=1 (pure water). For more detailed information and the derivation of the Forchheimer formulas

(e.g. continuity and momentum equations for porous medium) given below, one is refered to Appendix B.

$$\frac{\partial \zeta}{\partial t} = -\frac{\partial\left(\frac{q}{n}\right)}{\partial x}$$

$$\frac{1}{n}\frac{\partial u}{\partial t} + \frac{\frac{u}{n}\partial\frac{u}{n}}{\partial x} + g\frac{\partial \zeta}{\partial x} + \ldots + f_l u + f_t u|u| = 0$$

$$fl = \alpha_E \frac{(1-n)^3}{n^2}\frac{\nu}{d^2} \quad \text{and} \quad f_t = \beta\frac{1-n}{n^3}\frac{1}{d}I = \alpha\frac{\nu}{g}\left(\frac{u_k}{D^2}\right) + \beta\frac{1}{g}\frac{u^2{}_k}{D}$$

Where ζ denotes surface elevation, ν the kinematic viscosity and u the horizontal flow velocity, *D* is the grain size and g is the gravitational acceleration.

Advantages SWASH

SWASH improves its frequency dispersion by increasing the number of layers rather than increasing the order of derivatives of the dependent variables like Boussinesq type wave models. Yet it contains at most second spatial derivatives, whereas the applied finite difference approximations are at most second order accurate in both time and space. In addition, SWASH does not have any numerical filter nor dedicated dissipation mechanism to eliminate short wave instabilities. Neither does SWASH include other special measures like the surface roller model for wave breaking, in Zijlema and Stelling (2008) the authors showed that, when using momentum conservative numerical schemes as described in Stelling and Duinmeijer (2003), the effect of wave breaking can be captured accurately without the use of a breaking model. This is an advantage over Boussinesq models which generally need a separate breaking model to initiate the breaking process. As such, SWASH is very likely to be competitive with the extended boussinesq type wave models in terms of robustness and the computational resource required to provide reliable model outcomes in challenging wave and flow conditions.

3.3. Determine the reflection coefficient in SWASH and MIKE21

For Boussinesq wave simulation and for the non-hydrostatic approach, the equations in Mike21 BW and SWASH have been modified to include porosity and the effects of non-Darcy flow through porous media. In this way, it is possible for MIKE21 and SWASH to model partial reflection, absorption and transmission of wave energy at porous structures such as rubble mound breakwaters. For simulations of partial wave reflection and/or wave transmission through various types of structures one would need to create a porosity file. The porosity file includes a porosity, which is set to unity at open water points (no dissipation) and between 0.1 and 1 along structures where one wants to include the dissipation effect of porous flow.

The main effects of porosity are introduced by additional laminar and turbulent friction terms for describing losses due to flow through a porous structure. In most practical cases the pore size are relatively large (typically 0.1 m to 1.0 m), and the turbulent losses will dominate. The laminar loss term has also been included to allow the simulation of small scale physical model tests.

The flow resistance inside the porous structure is described by the non-linear term

$$U(\alpha + \beta|U|) = f\frac{\omega}{n}U$$

In which α and β account for the laminar and turbulent friction loss, respectively, U is the velocity, ω is the radian frequency and f is the friction factor. α and β are determined by the empirical expressions recommended by Engelund (1953):

$$\alpha = \alpha_0 \frac{(1-n)^3}{n^2}\frac{\nu}{d^2}$$

$$\beta = \beta_0 \frac{1-n}{n^3}\frac{1}{d}$$

Where:

n = porosity
ν = kinematic viscosity
d = a characteristic diameter of the structure units (grain size)
α_0 = a laminar particle form resistance coefficient
β_0 = a turbulent particle form resistance coefficient

The default value form SWASH and MIKE21 for α = 1000 and for β = 2.8.

There are differences between MIKE21 and SWASH in determining the reflection coefficient. In MIKE21 one should use the '*toolbox calculation reflection coefficient';* this tool can help to determine the porosity or friction factor to use in the wave simulation to obtain the desired reflection and/or transmission coefficient.

For this purpose one should specify the expected wave height, wave period and the water depth in front of the structure. In case irregular waves are used as input, one should take the wave height as the significant wave height. The wave period should be taken as the spectral peak wave period specified at the open boundary. In case one wants to calculate the friction coefficient only the water depth and wave period has to be determined.

The width of the absorber should correspond to the thickness of the porosity/friction layer used in the wave model set-up. The width should not be less than 25% of the characteristic wave length in order to be efficient. In practical short periodic harbour wave disturbance studies 3-5 porosity layers are typically used.

The output file will contain the reflection coefficient (and the transmission coefficient in case of permeable core). Also, the non-linear friction factor corresponding to the specified porosity is included in the output file.

As the reflective characteristics of an absorbing structure is mainly a function of the wave height, wave period and water depth, one should apply this this tool for a number of different combination of these parameters. This way, one can find the porosity/friction value for the desired reflection coefficient.

Typical example of the output of this tool is presented below:

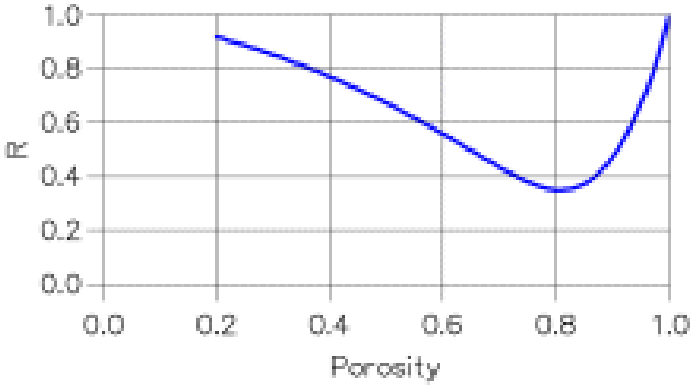

Figure 10: Reflection coefficient versus porosity. Conditions: Significant wave height=1m, spectral peak wave period = 9 s and water depth =10 m. the width of the absorber is 15 m and the core is impermeable, DHI (2008)

As from Figure 10 two different porosities may yield the same reflection coefficient. One should select the porosity which corresponds to the part of the curve with the mildest slope (e.g. use a porosity of 0.73 to obtain 40% reflection instead of 0.87). if, however, the desired reflection coefficient requires a porosity less than about 0.4, it is recommended to consider the steepest part of the curve.

In SWASH there is no toolbox to calculate the desired reflection beforehand. The reflection coefficient in SWASH can be determined by measuring the time series of surface elevation. The measured signal should decompose in incoming wave signal and reflected wave signal, after that the incoming and reflected wave heights can be determined. The incoming and reflected wave heights are obtained from the zeroth-order moment of decomposed signal, which is a result from the integration of the energy density spectra over a frequency range.

4. 1D simulations

4.1. Introduction

In this chapter the flow through porous structures will be studied using SWASH. The chapter is divided in two parts.

In the first part, SWASH results are compared with experimental data by Mellink (2012), analytical solutions performed by Madsen (1983) and empirical formulation by Seelig (1980). The results will give insight in the dependency of reflection coefficient on several physical parameters. As the reflection of wave through breakwaters depends on the wave conditions and breakwater geometry, it is valuable to gain insight in the model predictions for a range of conditions. Further, the reflection coefficient will be determined for different type of structures.

In the second part, the reflection and transmission of bound long waves will be studied. The results will give insight in the behaviour of bound and free long waves nearby breakwater. SWASH results are compared with experiment performed by Hossain et al (2001). They found from the experimental results that, although the breakwater can reflect short waves energy efficiently, a significant part of the bound long-wave energy is transmitted into the harbour basin as free wave through the breakwater. Different simulations are performed to indicate whether or not SWASH is capable to produce the same results.

This chapter is structured as follows: first the model setup and the important choices to setup the model are explained (4.2). The results of the first part are presented in (4.3). Model setup and the important choices to set up the model for the second part is explained (4.4). The results of the second part are presented in (4.5).

.

4.2. Reflection of monchromatic waves

In this part a description is given for the performed simulation by SWASH. The SWASH results are compared with experiment, analytical solutions and empirical formulations.

4.2.1. Model setup

The reflection coefficient is determined for several parameters. The influence of the porosity (*n*), wave period (*T*) and wave height (*H*) on the reflection is investigated. Figure 11 depicts the different types of structure for which, using SWASH, reflection coefficient will be determined.

Structure 1 is a schematization of rubble mound structure with impermeable core; the structure is represented by an imperious wall with a porous structure in front of it. Further, it is considered to be homogenous, rectangular and the bottom horizontal. From Section 2.2.1 it was shown that Madsen (1983) has derived for this specific case an analytical solution. This case will be set up in SWASH to compare both results with each other.

Structure 2 is also considered to be a homogeneous and rectangular, the water depth is assumed constant at both sides of the breakwater. For this structure an experiment has been performed at Technical University of Delft by Mellink (2012). The experimental results will be used to compare results from SWASH.

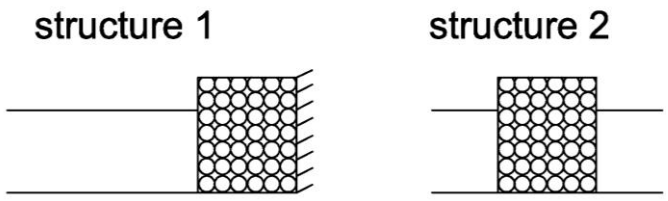

Figure 11: type of structures

4.2.2. Influence physical parameter on reflection

Madsen (1983) showed that the reflection coefficient is a function of porosity (*n*), the width of breakwater (*w*), incoming wave amplitude (*a*), diameter of stones/grains (*d*), water depth (*h*), friction factor (*f*) and the wave period (*T*). In this study a selection of physical parameter is made which can have large influence on the reflection. The parameters which are considered are the porosity (n), three different porosity are used, n=0.1, n=0.5 and n=0.9. The influence of the wave height is also studied, two different wave height are considered, H=0.5 m and H=1.5 m. Furthermore, the wave period is also considered for structures 1 and 2. For those structures relative long waves are taken into account, wave periods from 15 to 65 sec in water depth of 21 m are considered. The influence of each physical parameter and type of structure is investigated in separate cases (1 to 8). An overview of studied case are given in Table 4.

Table 4: parameters for studied cases

case	structure	n [-]	H [m]	T [s]	w [m]
1	1	0.5	0.5	15 to 65	100
2	1	0.1	0.5	17.3	0..200
3	1	0.5	0.5	17.3	0..200
4	1	0.9	0.5	17.3	0..200
5	1	0.5	1.5	17.3	0..200
6	2	0.5	0.5	15 to 65	100
7	2	0.5	0.5	17.3	0..200
8	2	0.5	1.5	20 to 60	100

The influence of each parameter is summarized here below

- Influence wave period structure 1 (case 1)
- Influence porosity structure 1 (case 2 to 4)
- Influence wave height structure 1 (case 3 and 5)
- Influence wave height structure 2 (case 6 and 7)
- Influence wave period structure 2 (case 8)

4.2.3. Computational domain

A sketch of the computational domain used for the simulations is shown in Figure 12. In addition, the choices that were made setting-up the model are explained in this section.

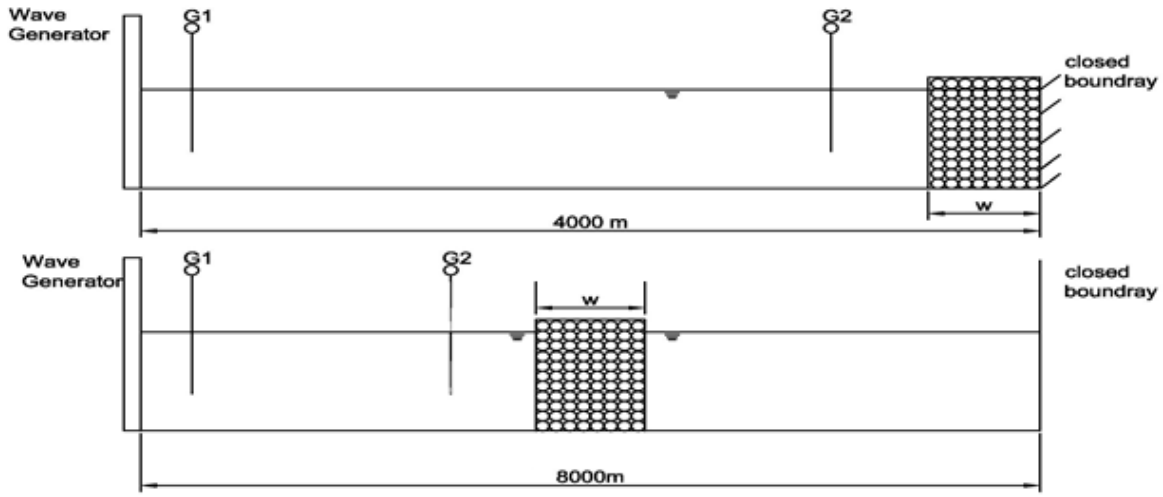

Figure 12 : Computational domain

4.2.3.1. Grid resolution

Based on the linear dispersion relation the shortest wave length is calculated. For all simulations the grid size was Δx=λ/50, where the wave length λ corresponds to the shortest wave length. For the simulation of structure 1 and 2 Δx=4 m is taken.

The time integration method of SWASH is explicit, which means that in order to end up with a stable computation the CFL condition has to be full filled.

$$C\,\Delta t / \Delta x < 0.4$$

Here c is the wave speed, for the simulations of structure 1 and 2, c=14.35 m/s is taken, which corresponds to a wave period of 15 sec, using the CFL condition a Δt = 0.11 sec is taken.

4.2.3.2. Boundary conditions

The 1D model has two boundaries, to simulate entering waves without reflections at the inflow boundary a weakly reflective condition allowing outgoing wave were used. A closed boundary is used at the end of the computational domain allowing waves to reflect for structure 1. For structure 2 a sponge layer is chosen which makes it possible that waves leave the computational domain without disturbing the measured signal. The length of the sponge layer is 3 to 5 times the wave length. For the simulations of structure 2 a sponge layer of 600 m is taken.

4.2.4. Method analysis

The reflection coefficient was defined as follow

$$R = \frac{H_r}{H_i}$$

Where H_i= wave height of reflected wave and H_r=wave height of incident wave. Two wave gauges were used for the simulations. One wave gauge was placed in the front of the wave maker and the other one near the breakwater. To determine the incoming and outgoing components the signal was decomposed using the collocated method. With the collocated method the decomposition is carried out in the time domain, using the surface elevation and velocity signal at the same location (collocated sensor). The collocated method is only applicable for long waves, for more detailed information and the derivation of the separation method; one is referenced to Appendix C.

After the signal is separated in incoming and outgoing component, the incoming and outgoing wave heights are obtained from the zeroth-order moment of decomposed signal, which is a result from the integration of the energy density spectra over a frequency range. The energy density spectra are obtained with the Fourier transform.

4.3. Results

In this section the reflection coefficient is shown as a function of the wave period, width of the breakwater, the porosity and of the incoming wave height. The SWASH results are compared with analytical solution Madsen (1983) for case 1 to 5. Further, case 6 and 7 are compared with experimental results performed at Technical university of Delft and the last case 8 is compared with empirical formulation performed by Seelig (1980).

4.3.1. Influence wave period case 1

In Figure 13 the reflection coefficient is shown as a function of the wave period (*T*). SWASH results shows almost a perfect fit with the analytical solution performed by Madsen (1983). This was expected, because the formulas that are implemented in SWASH to calculate the porous flow are the same as the formulas derived by Madsen (1983). From Section 3.2.2 it was shown that SWASH uses the Forchheimer equation in describing porous flows. The analytical solution described by Madsen (1983) also uses the Forchheimer equation as shown in Section 2.2.1. The difference between the analytical model and SWASH is that the analytical model used linearized friction instead of nonlinear friction implement in SWASH. This difference is insignicant as the SWASH results and fit very well with the analytical solution.

Further it is interesting to see that the wave period has a large influence on the reflection. The reflection coefficient is almost 30 percent smaller for a wave period of 25 sec compared with a wave period of 15 sec. This means, one can investigate the most efficient situation of breakwater width and wave length to reduce the wave penetration in harbours as much as possible.

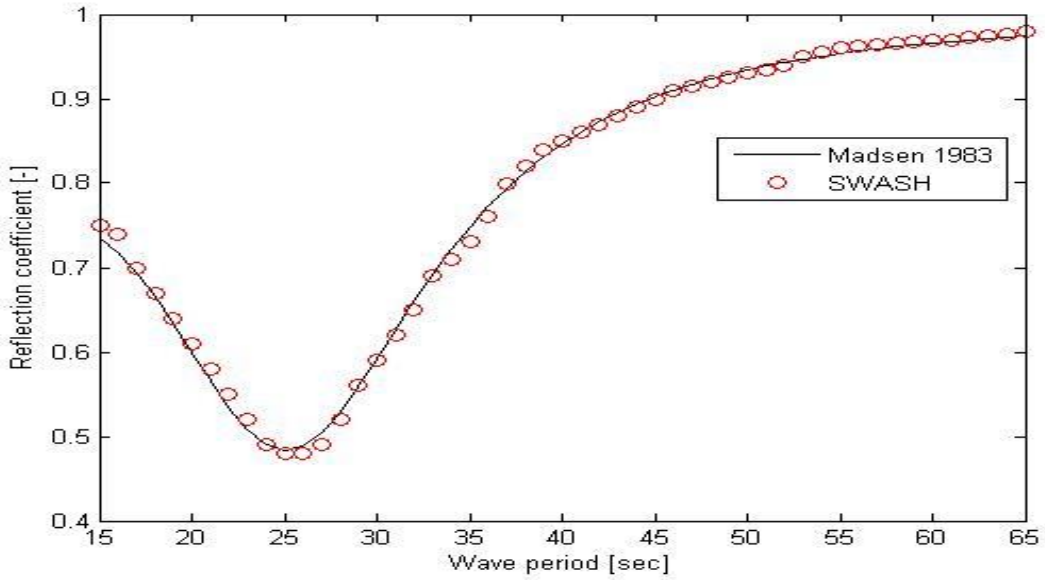

Figure 13: Reflection coefficient as function of the wave period; a comparison between Madsen (1983) and the results generated using SWASH

A possible declaration for the deflection near the wave period of 25 sec is that the system is not enough damped . Madsen (1983) has described a method to determine the friction coefficient as a function of the wave height, see section 2.2.1.1. The same method by Madsen (1983) is followed to determine the friction coefficient for this case (e.g. *H*=0.5). The applied method gives a friction factor

value of 0.2. A second calculation has been performed with a wave height of 1.5 m and this give a friction factor of 4. The relative larger value of the friction coefficient provides more damping and that ensures that the solution stay stable. For all values of *T*, the reflection coefficient has almost a value of 0.7 and the deflection is diminished.

The variation of the reflection coefficient with *T* for different wave heights (*H*=0.5 and *H*=1.5 m) is presented in Figure 14.

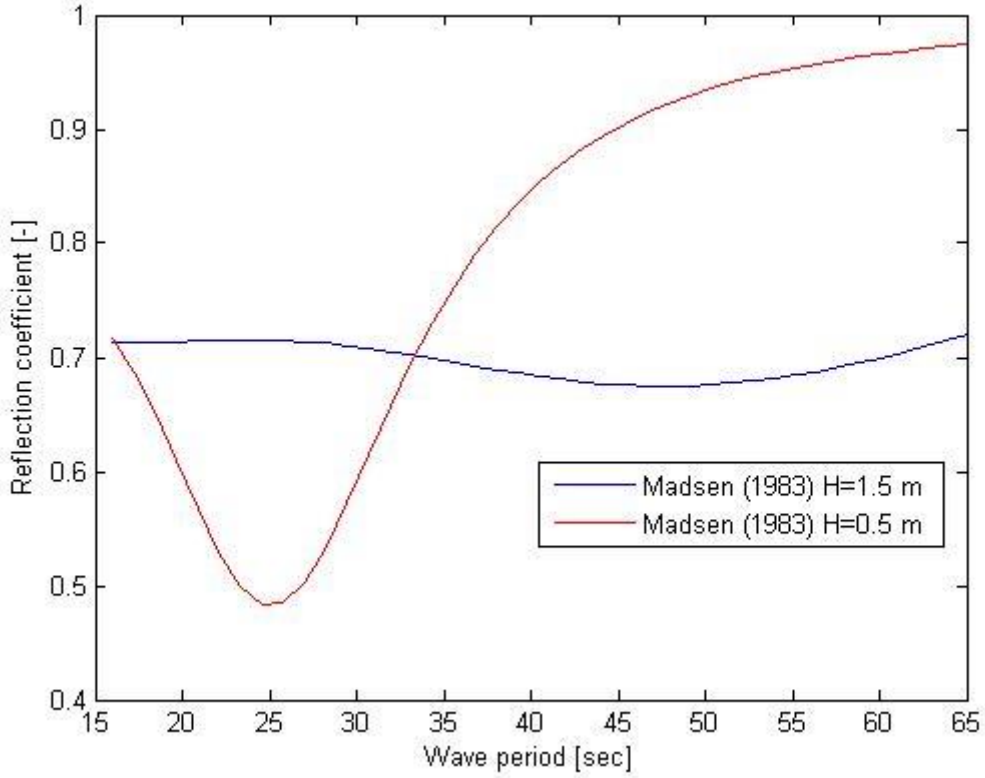

Figure 14:Reflection coefficient as function of the wave period (H=0.5 m and H=1.5 m); according Madsen (1983).

4.3.1. Influence porosity (case 2 to 4)

In Figure 15 the reflection coefficient is shown as a function of the width of the breakwater (*w*) relative to the wave number (*k*) for structure 1. The porosity has large influence on the reflection. The solution has an oscillatory character when the porosity is equal to 0.5. The oscillation is less visible for more porous breakwater (i.e. *n*=0.9) and totally diminished when the breakwater is very impermeable breakwater (i.e. *n*=0.1).

An interesting case is when the breakwater is semi-permeable (i.e. *n*=0.50) and a width which is 2 times larger than the wave length (i.e. *kw*=2). In that case, the reflection is significantly smaller when it is compared to breakwater with a width 3 time larger than the wave length (i.e. *kw*=3). Because of the oscillatory behaviour for when n=0.5, it appears that a long breakwater does not necessarily absorb more energy than a shorter one. In the case the breakwater width is in the same order of the wave length (i.e. kw=1), the breakwater will almost fully reflect the waves. Concluding from this, for this case, the most efficient ratio between the breakwater width and wave length is kw=2. For this ratio between the width and wave length relative large amount of energy is dissipated, which also means the wave penetration in the harbour basin will be significantly smaller than kw=1 and kw=3. The rubble mound breakwaters used in practical application have almost a porosity between 0.4 to 0.5, this is why a porosity of 0.5 is taken for the next cases to study the reflection behaviour.

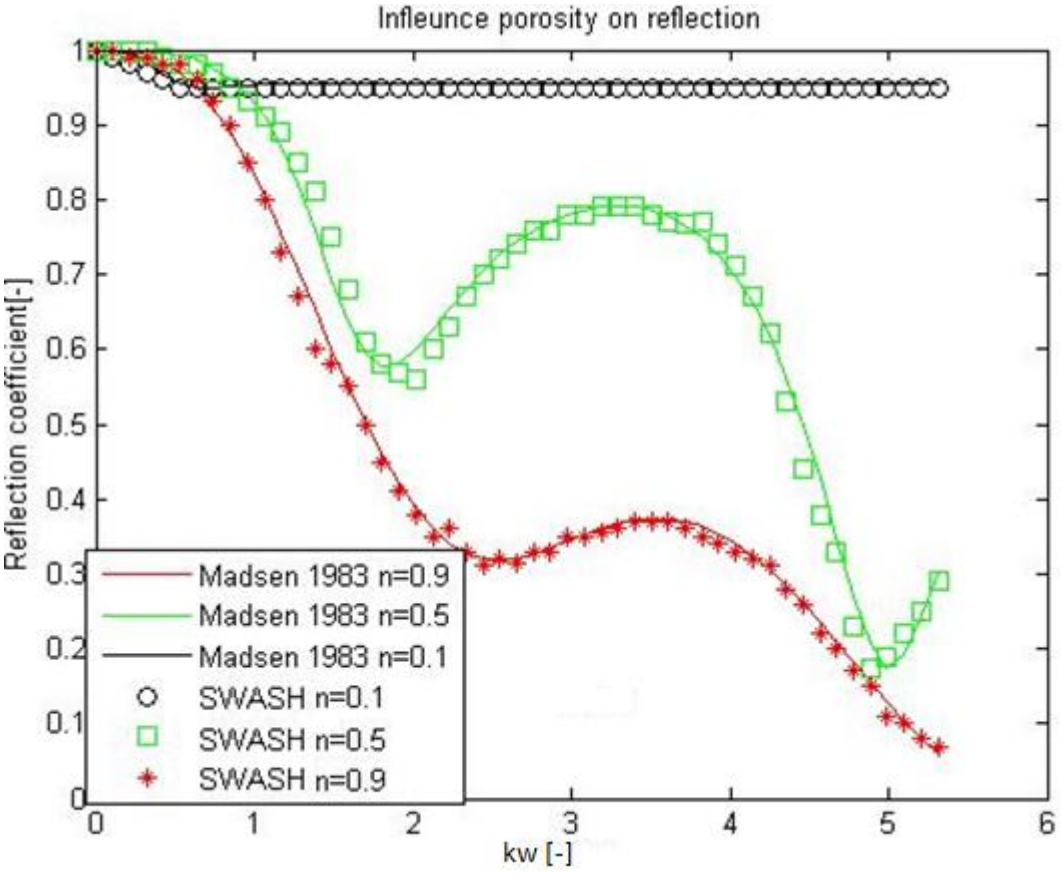

Figure 15: Reflection as function of breakwater width multiplied with wave number; influence of porosity

4.3.2. Influence wave height (case 3 and 5)

In Figure 16 the reflection coefficient is shown as a function of the width of the breakwater (*w*) relative to the wave number (*k*). SWASH results shows almost a perfect fit with the analytical solution performed by Madsen (1983). The wave height has large influence on the reflection. The solution has an oscillatory character for wave height H=0.5 and for a wave height of H=1.5 the oscillatory behaviour is negligible. It appears that the reflection coefficient can be considered constant for *kw* values larger than 0.8. For a wave height H=1.5 m, the value of the reflection coefficient varies between 0.7 and 0.8 . The value of *kw* has minor effect on the reflection coefficient when the wave height is equal to 1.5 m, while for H=0.5 m the energy absorption strongly depends on the ratio between the breakwater width and the wave length.

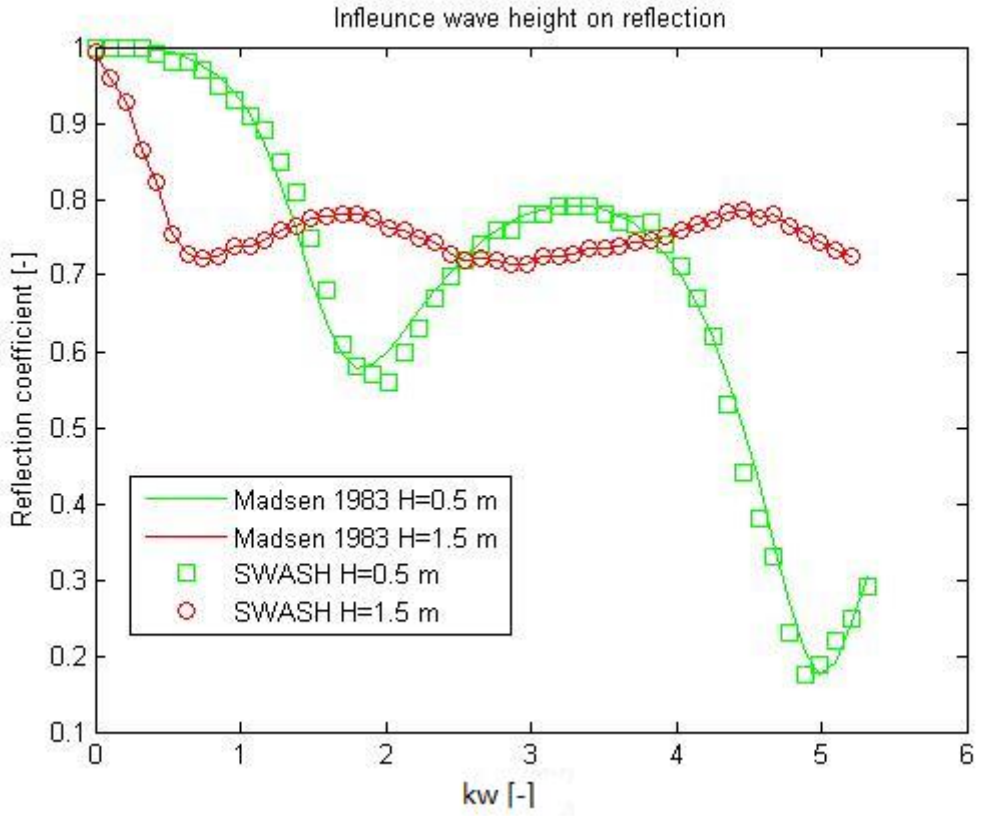

Figure 16: Reflection as function of breakwater width multiplied with wave number; influence of wave height

Also here the reason for the oscillatory behaviour seems the low friction factor for the wave height of 0.5 m (e.g. *f*=0.20), whereas relative larger wave height *H*=1.5 (e.g. *f*=4) convergence to a fixed value. The variation of the reflection coefficient with *kw* for different values for the friction factors (*f*=0.15, *f*=1.0 , *f*=7.0 , *f*=8.0) is presented in Figure 17. The reflection coefficient exhibit an oscillatory nature for the friction factor of 0.15 over the entire range of *kw*. For higher values of *kw*, the reflection coefficient increases with higher friction factor and the oscillatory nature is diminished.

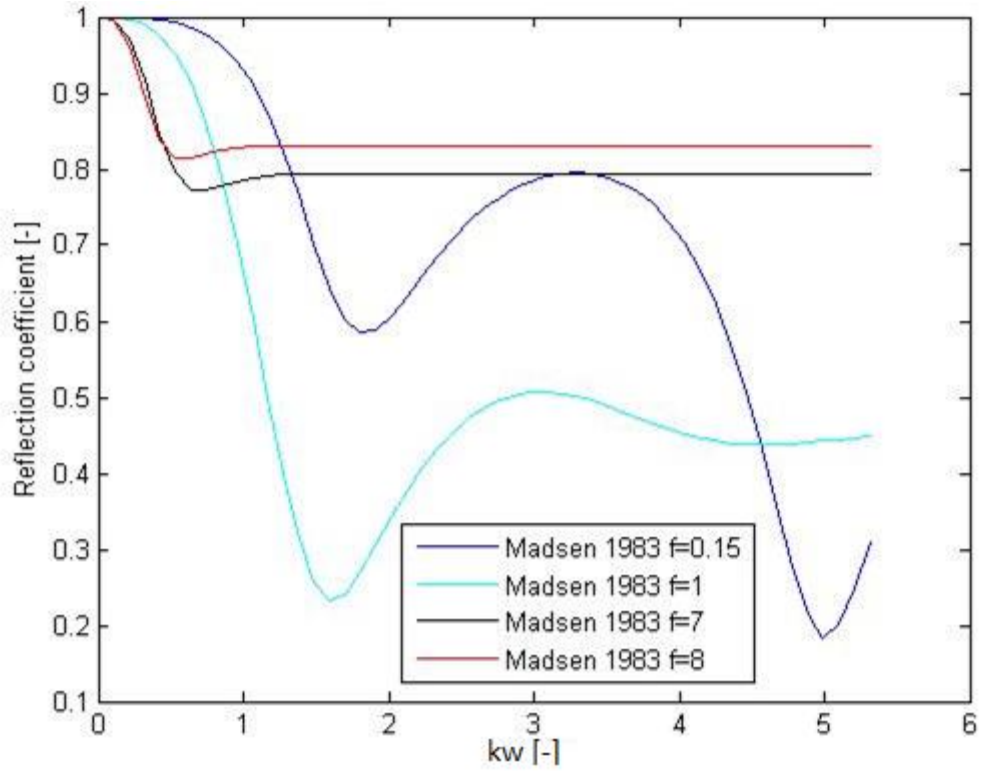

Figure 17: Influence friction factor on reflection according Madsen (1983).

4.3.3. Effect of wave height on the reflection coefficient for structure 2 (case 6 and 7)

In Figure 18 the reflection coefficient is shown as a function of the width of the breakwater (*w*) relative to the wave number (*k*). SWASH results are compared with experimental data obtain by Mellink (2012). Mellink used a wave height of 0.1 m through the experiment which corresponds with a wave height of 1.5 m in prototype scale. The experiment performed by Mellink (2012) covers only the first part in the graph as the experiment were naturally limited by small *kw* values. The results show good agreement with the measurement the deviations are less than 10 percent without any calibration of the model. For structure 2 it is also seen that the behaviour of the reflection strongly depended on the wave height. For relative small waves the solutions gives an oscillatory behaviour, while for a larger wave height (i.e. H=1.5 m) the solution is almost constant after kw=0.5.

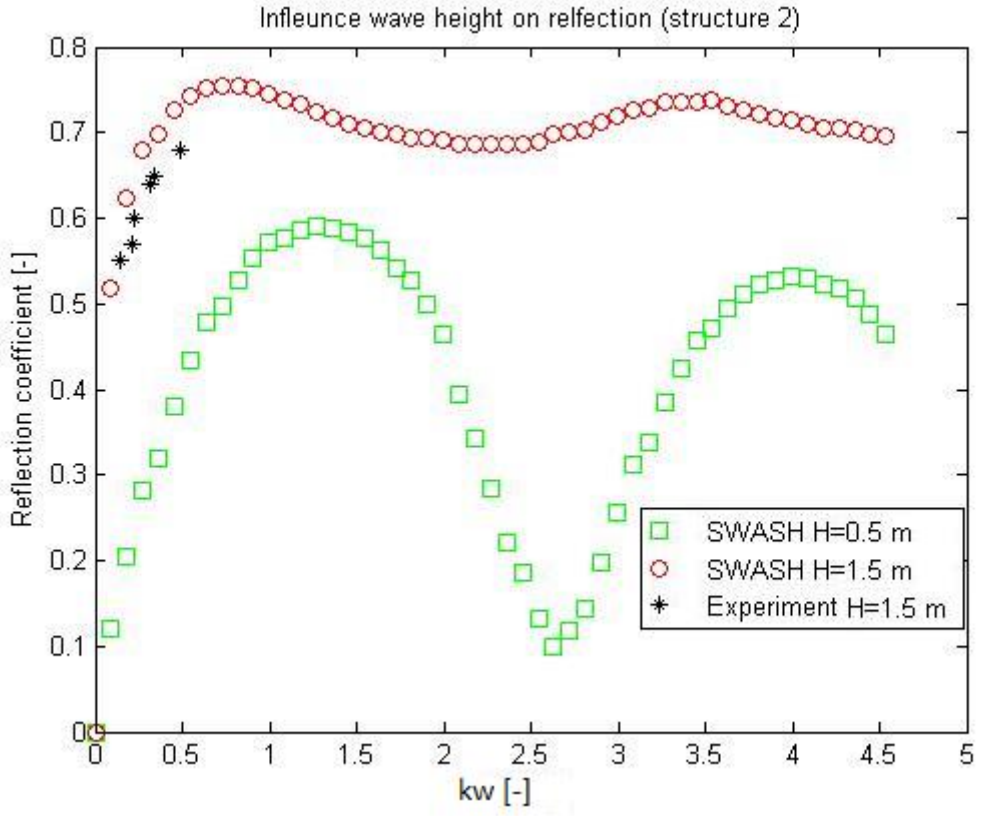

Figure 18: Reflection as function of breakwater width multiplied with wave number; influence wave height structure 2

4.3.4. Effect of wave period on the reflection coefficient for structure 2 (case 8)

In Figure 19 the reflection coefficient is shown as a function of the wave period. SWASH results show almost perfect fit with the empirical results performed by Seelig (1980). The formulation of Seelig (1980) was derived from measurement of the sloped geometry. Unlike Seelig (1980), the tested case (structure 2) has a vertical porous breakwater. Due to the relative large wave length used in the simulation the influence of sloped is minimized. This is why the vertical breakwater used in SWASH can be compared with empirical results performed by Seelig (1980).

The empirical formulation by Seelig (1980) is based on rubble mound breakwaters, which almost have a porosity of 0.4, this why a porosity of 0.4 was chosen for the SWASH simulations. For a porosity n=0.4, the value of the reflection coefficient varies between 0.5 and 0.6 for the considered range of wave periods.

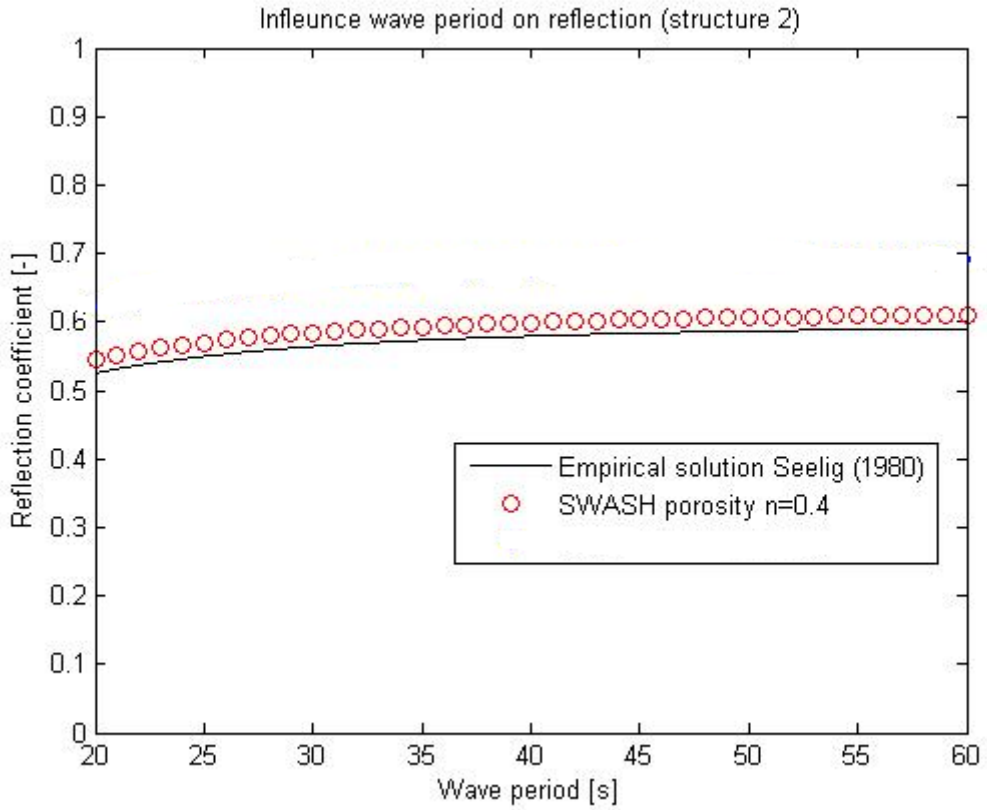

Figure 19: Reflection as function of breakwater width multiplied with wave number; influence wave period structure 2

4.4. Reflection and transmission Bichromatic waves

4.4.1. Model set-up

A sketch of the computational domain and the experimental setup is shown in Figure 20. From the figure one can see that the breakwater used in the experiment differs from the model setup. Hossain et al. (2001) used a breakwater composed of two different porosities: the upper part was impermeable, (i.e. porosity n=0) and the lower part had a porosity of n=0.45. However, in SWASH it is not possible to vary the porosity in vertical direction. A uniform porosity of n=0.20 is chosen for the simulations in SWASH. The porosity used in SWASH is based on the average value,

$$A/B \times C + D/B \times E = F$$

In which,

A = impermeable part height, B=Total height, C= porosity impermeable part, D = permeable part height, E= porosity permeable part, F=averaged value used in SWASH

$$(0.24/0.4) \times 0 + (0.16/0.4) \times 0.45 = 0.20$$

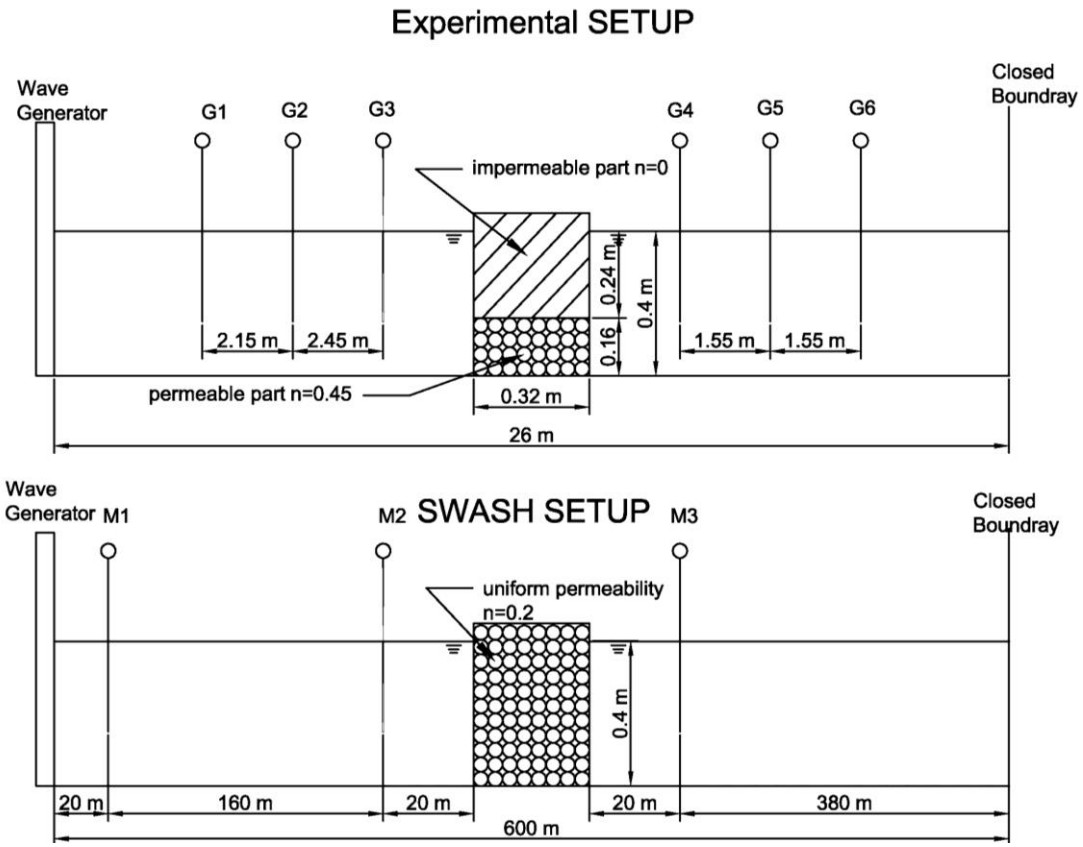

Figure 20: experimental setup; SWASH computational domain

.

4.4.2. Grid resolution

An important aspect of specifying a computational grid is the spatial resolution. The most energetic wave component (shortest wave) needs to be resolved accurately. For low waves that is a/h <<1, it is sufficient to take 50-100 grid cells per wave length. The grid definition in vertical direction is defined by means of a fixed number of layers in such way that the bottom topography and the free surface can be accurately represented. The number of layers is determined by the linear frequency dispersion. The higher the value of relative depth (kh), the more layers that are needed. The range of the kh value for the simulations was between 0.68 and 1.47. Two vertical layers were used to obtain good dispersive properties for the kd values that were encountered. A base time step, dt=0.001 is used in order to fulfil the CFL condition.

4.4.3. Boundary conditions

Due to nonlinearity, sub and super waves are generated. To minimise the higher order harmonics, linear wave conditions are enforced at the inflow boundary. In order to satisfy the linear boundary condition, the model will generate free long components with the same magnitude, but 180 degree out of phase with the bound waves at the wavemaker. The presence of bound and free waves that travel at different phase speed will lead to disturbance in the wave field over the domain. For all simulations, command ADDboundwave was used to reduce this effect. The effect of the command ADDboundwave on wave field is shown in Figure 21.

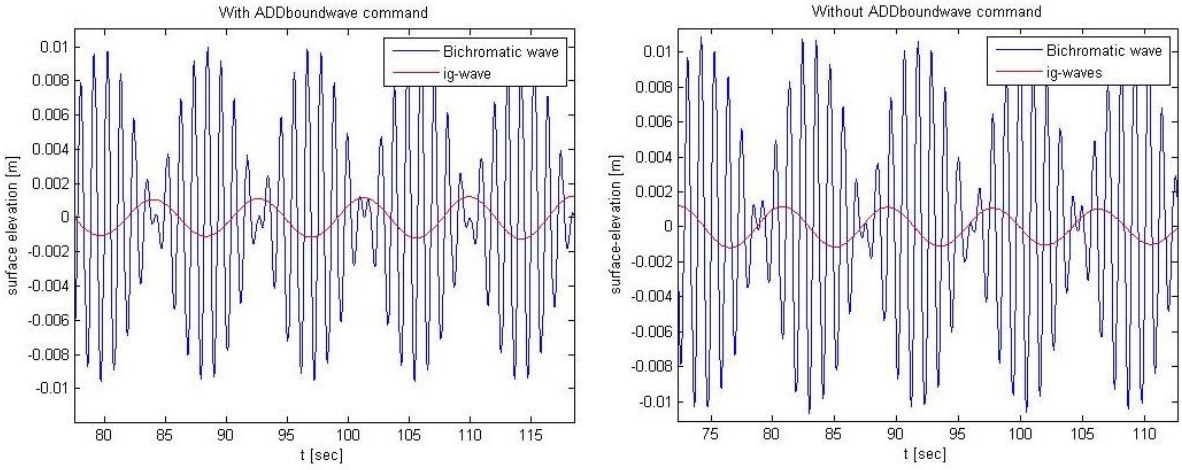

Figure 21: effect of ADDboundwave command

4.4.4. Wave conditions

Hossain et al (2001) conducted a total of ten different experiments varying the central wave period from 1.1 to 2.0 sec, which covers the relative depth kh from 0.68 to 1.47. The central wave period is defined as the average value of the first and second short wave periods, (T1+T2)/2 and the central wave number is defined as the average value of the first and second short wave numbers, (k1+k2)/2. The used depth in the experiment was 0.4 m. For the simulations in SWASH the wave conditions were taken the same as used in the experiment. An overview of the different wave conditions used in the experiment and simulations is given in Table 5.

Table 5:wave conditions experiment and SWASH simulations

Experiment and SWASH simulations			
simulation	**T1**	**T2**	**kh**
1	1.03	1.17	1.47
2	1.13	1.27	1.28
3	1.21	1.39	1.14
4	1.3	1.5	1.04
5	1.38	1.62	0.95
6	1.46	1.74	0.88
7	1.55	1.85	0.82
8	1.64	1.96	0.77
9	1.74	2.06	0.72
10	1.83	2.17	0.68

4.4.5. Method of analysis

In this section the analysis method is explained to determine the reflection and transmission coefficient.

Hossain et al (2001) defined the reflection and transmission coefficient as follow:

$$R = a_r/a_i \quad \text{and} \quad T=a_t/a_i$$

Where a_i = amplitude of incident bound long wave, a_r = amplitude of reflected free long wave and a_t= amplitude of transmitted free long wave. They found that a significant part of the energy of the bound waves is formed in free long wave energy after the bound waves reach the breakwater. This is the reason why they could neglect the reflected/transmitted bound long wave from their analysis without any major effects.

Amount of bound and free energy

The findings by Hossain, Kioka et al. (2001) are based on breakwater geometry shown in Figure 20. To analyse if this also holds for the breakwater used in SWASH, simulations are performed which show the amount of bound and free energy before and after the waves reach the breakwater. To differentiate between the free and bound component, the same method used by Rijnsdorp et al. (2014) was also applied in this case. This analysis is based on the difference in wave length between the bound and free component: the length of the bound waves is the difference wave number k_b = *k1* **–k2** ; herein is *k1* and *k2* the wavenumbers of the short wave components. The free wave number k_f follows from the difference frequency f_{ig} = f2 –f1 and the linear dispersion relationship. The energy of ig-wave component was estimated from the wave number spectrum E(k)

$$E_{ig} = \int_{k_{lo}}^{k_{hi}} E(k)dk$$

Where k_{hi} and k_{lo} are the higher and lower limit of the wave number band.

4.4.6. Filtering and Separation signal

The signal has been divided into short wave and ig-wave components. This has been done to distinguish between the reflection and transmission of short waves and IG-waves components. The frequency bands for the short wave were $0.95 f_1 \le f_{sh} \le 1.05 f_1$ herein, and for the IG-waves $0.95 f_b \le f_{ig} \le 1.05 f_b$ these frequency bands contain the energy of respective components.

Where f1 = frequency of the first short wave component, f_{ig} = frequency of the IG-wave and f_b = frequency bound waves

To determine the incoming and outgoing component the signal was decomposed using the collocated method. The decomposition is carried out in the time domain, using the long wave surface elevation and long wave velocity signal at the same location. The incoming ig- component and outgoing ig-component is shown in Figure 22.

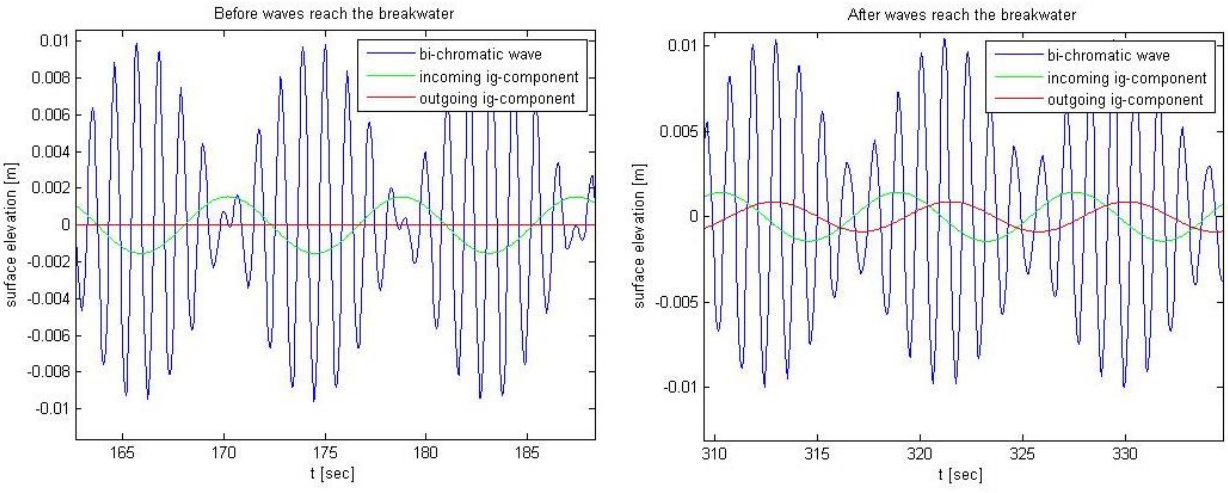

Figure 22: decomposed signal before and after waves reach the breakwater

The incoming and outgoing wave heights were obtained from the zeroth-order moment of decomposed signal, which is a result from the integration of the energy density spectra over a frequency range. The energy density spectra are obtained using fast Fourier transforms.

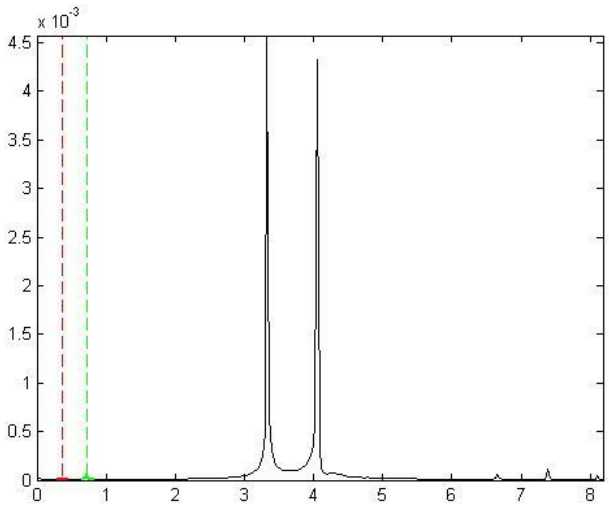

Figure 23: The estimation of the ig-wave energies from the wave number spectrum.

4.5. Results

As stated before there are different simulations performed to compare the results showed by Hossain et al (2001) to SWASH simulations. Below the results of the following simulation are presented.

1. Transmission short waves forced by bi-chromatic waves
2. Reflection and transmission IG-waves forced by bi-chromatic waves
3. Distribution bound vs free energy before and after waves reach the breakwater

4.5.1. Transmission short waves forced by wave groups

Comparison between measured and SWASH result for transmission coefficient for short waves is presented in Figure 24. Both results disagree with each other; the transmission for the SWASH simulations is smaller than the performed experiment. This means that the flow experience high resistance in the porous part, the breakwater that was chosen for the SWASH simulation instead of the original breakwater show unreliable results. Also there is not a comparable trend found between the SWASH results and experiment. The experiments results show that the amount of transmission decreases for larger *kh* values, while the SWASH results shows almost a constant value for the transmission.

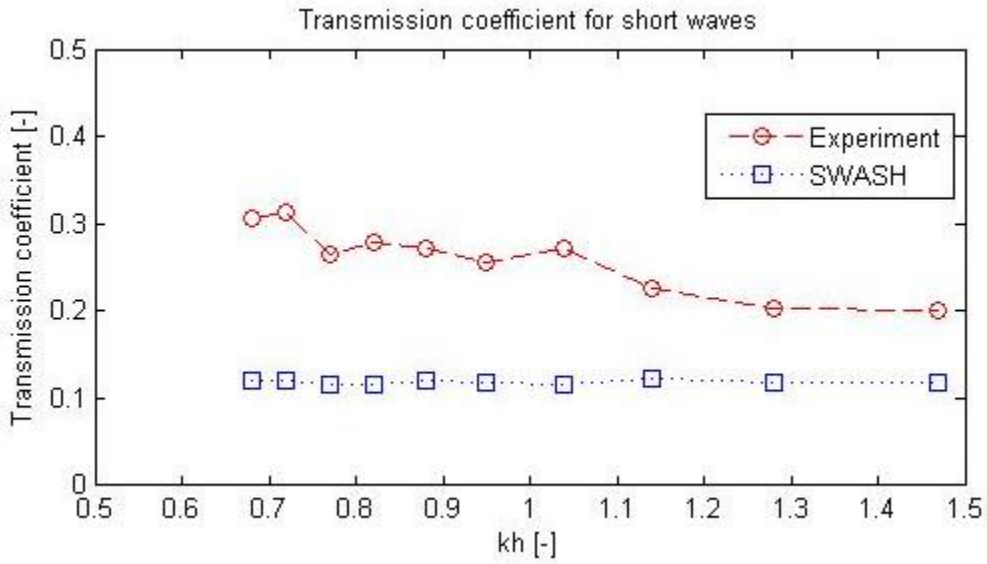

Figure 24: Transmission coefficient short waves experiment and SWASH

4.5.2. Reflection IG-waves induced by short waves

Comparison between measured and SWASH result for reflection of IG-wave is presented in Figure 25. The results for the reflection of IG-waves agree fairly well with each other. All swash values are within the boundary of the confidence interval of 15 percent. With the large difference between the breakwater used in the experiment and SWASH simulations is this quit good result. Furthermore a positive remake is that the SWASH results show similar trend as the experimental results. To converge the SWASH result to the experiment by varying the porosity of the breakwater used in the SWASH simulations, will not make sense, because some value of SWASH are higher than the experiment and some other lower.

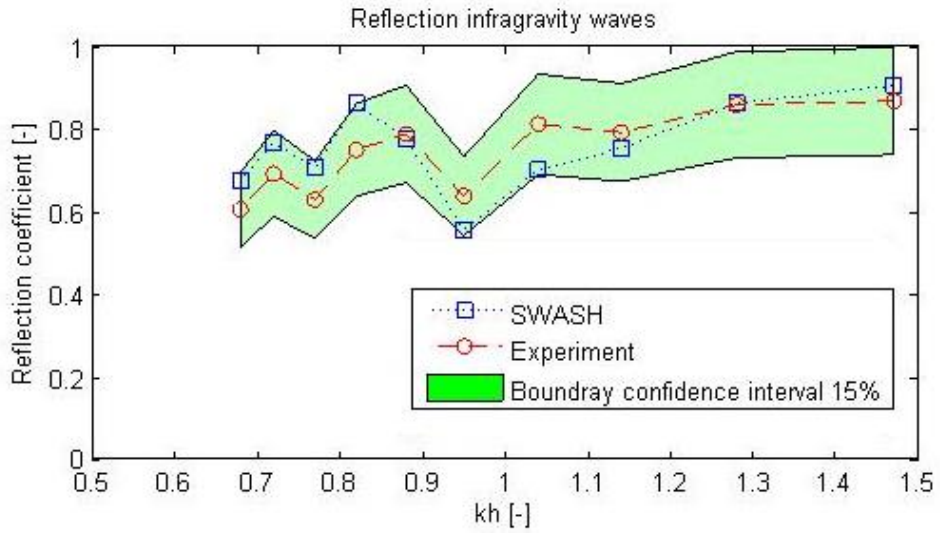

Figure 25: reflection ig-waves experiment and SWASH

4.5.3. Transmission infragravity waves induced by bichromatic waves

Comparison between measured and SWASH result for transmission of ig-wave is presented in Figure 26. The results are not satisfactory, because the transmission is greatly underestimated. The transmission coefficient found in the experiment is around or larger than 0.8. This indicates that a significant part of the energy of bound waves associated with the incident wave groups is transmitted to the leeward side of the breakwater. In addition no comparable trend was found between the SWASH results and the experiment. The experiment shows that more waves are transmitted for larger kh values; this trend is not seen back in SWASH results.

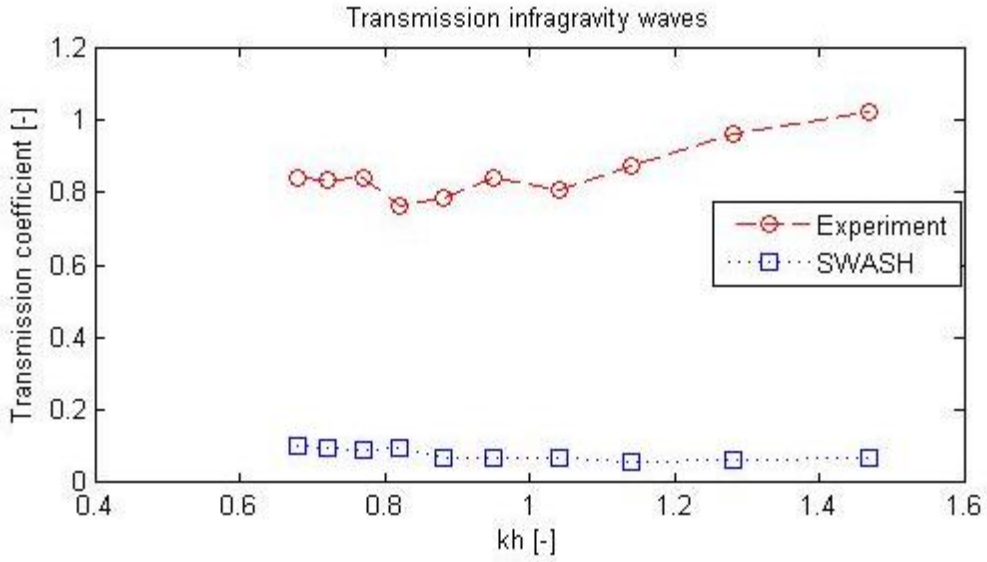

Figure 26: transmission coefficient ig-waves experiment and SWASH

The results above show that the reflection of the IG-waves are good in agreement with the experimental result, but the transmission of the IG waves show large deviation from the performed experiment. The reason with large deviation could be the difference in breakwater geometry between the used breakwater in SWASH and the experiment.

The SWASH results underestimate the transmission in comparison with the experiment results. This means that the flow has large resistance in the porous part, which indicate that the friction in the porous part is significant overestimated. By varying the laminar and turbulent particle resistance coefficient (α_0 and β_0), it is possible to shift the SWASH values towards the experiment values. A remarkable point if the results are shifted towards the experimental values than the sum of the transmission and reflection coefficient will be large than 1. This result is not realistic, since the sum of the reflection, transmission coefficient and dissipation must be always smaller than 1.

5. Conclusion and recommendations

The objective of this thesis was to establish the influence of several physical parameters on reflection of monochromatic waves for different type of structures. For this purpose simulations have been performed with SWASH and the results are compared with experimental data, analytical solutions and empirical formulations. The model predictions are found to be consistent with lab experiment, analytical solution and empirical formulation. A second objective was to investigate the capability of SWASH in predicting reflection and transmission of breakwater for irregular (bi-chromatic) waves. SWASH showed good results for the reflection of bound long waves, but the transmission of the primary waves and bound long waves were inconsistent with the experimental results.

5.1. Conclusion

In the first part of this study the influence of wave conditions and breakwater characteristics on the reflection is studied. In a number of cases the influence of the porosity, wave height and wave period and the width of the breakwater were considered. When the SWASH results are compared with the analytical solution in Madsen (1983), one can conclude that the porosity, wave height and wave period have large influence on the reflection. A breakwater porosity of 0.5 shows a strong oscillatory behaviour when the breakwater was forced with a wave height of 0.5 m. That is an interesting result, because it appears that a longer breakwater does not necessarily absorb more energy than a shorter one. In practice this can be used to find an efficient ratio between the breakwater width and wave length to reduce the building cost of the breakwater, while the breakwater capability in energy dissipation will remain the same.

But, the oscillations in the reflection coefficient were found to be strong related to the wave height. A relative large wave height (e.g. 1.5 m) give a high value for the friction factor. This cause that the solution is damped out and converge to a fixed value. In practical application this will be always the case, the wave height of 1.5 m is very common and one should design the breakwater according to this assumption. Although, the oscillatory behaviour for the small wave height seem very attractive, since the designers could adapt the breakwater width to reach the most efficient situations. It is not realistic, since the decisive value should be taken and this will be always larger than 1.5 m.

The convergence of the solution to a fixed value is also confirmed by the empirical formulation Seelig (1980) and the experiment performed by Mellink (2012). Unfortunately, there were no experiments available that covered a large range of *kw* value. The experiment performed by Mellink (2012) covers only small kw values. However, the results by Mellink (2012) are in concordance with the results of SWASH for the small *kw* values. The agreement between is promising, but to ensure that the reflection coefficient will converge to a fixed value experiment with larger *kw* values should be performed. It is difficult to perform experiments which cover a large *kw* values, since relatively long waves will be used and most often the flumes have a limited length. To overcome this problem one can take a small constant wave length and only vary the breakwater width in order to reach the large *kw* values.

Furthermore, both Type of structures 1 and 2 showed no difference in behaviour, both structures showed oscillatory behaviour of relative small wave height and more constant value for larger wave heights.

In the second part, a comparison between experimental and SWASH results were performed for the reflection and transmission of IG-waves induced by the short-wave groups due to vertical breakwater. The objective of the simulation was to indicate if SWASH is capable to produce comparable results as the experiment performed by Hossain et al (2001), due to the difference in breakwater geometry a perfect fit between the experimental and SWASH results was not expected.

The model predictions on the reflection of the bound long waves are found to be consistent with lab experiments. The model prediction deviates not more than 15 percent of the experimental results. On the other hand, the transmission of short waves and bound long waves were inconsistent with lab experiment. The results for the transmission of short waves and IG-waves showed a lower value of the transmission of all kh values. A explanation for this inconsistency is the large deviation between the breakwater geometry used in SWASH and the experiment. The SWASH results underestimate the transmission in comparison with the experiment results. A second possible explain is that the flow experience large resistance in the porous part, which indicate that the friction in the porous part is overestimated.

5.2. Recommendations

To investigate the reflection behaviour for large *kw* values experiments should be performed. As mentioned earlier it is rather difficult to perform this kind of experiments, because very large wave flumes are required to get the large *kw* values. To overcome this practical problem, it is advised to take a fixed short wave length and vary the width of the breakwater to reach the large *kw* values. Considering a field case with a water depth h =21; a wave period T=25 sec and breakwater width of w= 40 m, for this case a *kw* of 0.8 can be calculated. So, it is irrelevant to perform experiments with a *kw* value larger than 1. To reach this value the wave periods used by Mellink (2012) can be used, but the breakwater width should be doubled instead of 0,24 one should take a breakwater width of 0.48 m. The porosity of the breakwater should be taken as close as possible to the reality (e.g. n=0.4). Further, it is recommended to use two different waves heights, to study the influence on wave reflection. For this purpose the wave height by Mellink (2012) can be used. Besides, the wave heights used by Mellink it is advised to use very small wave heights (e.g 0.03 m) to determine the influence on the friction factor.

Further it is recommended to perform experiments with multi-layer structure to validate SWASH. In this thesis only simulations were performed with simple uniform single layer structures. To investigate if the model also works for a more complex (real life situations) those experiments are necessarily.

To be able to validate the transmission of short waves and ig waves in SWASH, it is highly recommended to perform experiments with a model with uniform porosity. In that case a fair comparison can be made. Another possible solution is to implement a new code in SWASH to simulate different porosities in the vertical direction. It is possible to use the performed experiment by Hossain et al (2001) to validated SWASH on transmission of short and ig waves. The implementation of different porosities in vertical direction is also important to create a sloped multi-layered structure, like a real breakwater in practical application. In order to use SWASH in practical cases, the implementation of different porosities is essential.

.

Bibliography

Battjes, J. A. (1974). Surf similarity. *Coastal Engineering Proceedings*, *1*(14).

Bowers, E. C. (1977). Harbour resonance due to set-down beneath wave groups. Journal of Fluid Mechanics, 79(01), 71-92.

CHEN, G. Y., CHIEN, C. C., SU, C. H. & TSENG, H. M. 2004. Resonance induced by edge waves in Hua-Lien Harbor. Journal of oceanography, 60, 1035-1043.

DHI (2005). Mike21 Boussinesq wave module: Short description. Hørsholm, Denmark.

Gunbak, A. R., & Brunn, P. M. (1979). Wave mechanics principles on the design of rubble-mound breakwaters. *Proc. Port and Oc. Engrg. Under Artic Conditions POAC*, *79*, 1301-1318.

GUZA, R., THORNTON, E. & HOLMAN, R. Year. Swash on steep and shallow beaches. In: Coastal Engineering, 1984 Houston. ASCE, 708-723.

Holthuijsen, L. H. (2007). *Waves in oceanic and coastal waters*. Cambridge University Press.

Hossain, A., Kioka, W., & Kitano, T. (2001). Transmission of long waves induced by short-wave groups through a composite breakwater. *Coastal Engineering Journal*, *43*(02), 83-97.

Journèe, J. M., & Massie, W. W. (2001). Offshore Hydrodynamics. *Delft University of Technology*, *4*, 38.

Kirby, J. T., Wei, G., Chen, Q., Kennedy, A. B., & Dalrymple, R. A. (1998). Funwave 1.0, fully nonlinear boussinesq wave model documentation and user's manual. *Center for Applied Coastal Research, University of Delaware*.

Madsen, O. S., & White, S. M. (1976). WAVE TRANSMISSION THROUGH. TRAPEZOIDAL BREAKWATERS. *Coastal Engineering Proceedings*, *1*(15).

Madsen, P. A. (1983). Wave reflection from a vertical permeable wave absorber. *Coastal Engineering*, *7*(4), 381-396.

Madsen, P. A., Murray, R., & Sørensen, O. R. (1991). A new form of the Boussinesq equations with improved linear dispersion characteristics. *Coastal engineering*, *15*(4), 371-388.

Mellink, B. (2012). Numerical and experimental research of wave interaction with a porous breakwater.

Miche, A. (1951). Le pouvoir r {é} fl {é} chissant des ouvrages maritimes expos {é} s {à} l\'action de la houle. *Annales des Ponts et Chauss {é} es*, *121*, 285-319.

Moraes, C. D. C. (1970). Experiments of wave reflexion on impermeable slopes. In *Coastal Engineering (1970)* (pp. 509-521). ASCE.

NACIRI, M., BUCHNER, B., BUNNIK, T., HUIJSMANS, R. & ANDREWS, J. Year. Low frequency motions of LNG carriers moored in shallow water. In: Offshore mechanics and Arctic Engineering, 2004 Vancouver, Canada.

Nwogu, O. G., & Demirbilek, Z. (2001). *BOUSS-2D: A Boussinesq wave model for coastal regions and harbors* (No. ERDC/CHL-TR-01-25). ENGINEER RESEARCH AND DEVELOPMENT CENTER VICKSBURG MS COASTAL AND HYDRAULICSLAB.

Rijnsdorp, D. P., Smit, P. B., & Zijlema, M. (2014). Non-hydrostatic modelling of infragravity waves under laboratory conditions. *Coastal Engineering*, *85*, 30-42.

Ursell, F., Dean, R. G., & Yu, Y. S. (1960). Forced small-amplitude water waves: a comparison of theory and experiment. *Journal of Fluid Mechanics*, *7*(01), 33-52.

Seelig, W. N. (1980). "Two-dimensional tests of wave transmission and reflection characteristics of laboratory breakwaters." *CERC Technical Report No. 80-1*, U.S. Army Waterways Experiment Station, Coastal Engineering Research Center, Fort Belvoir, Va

Seelig, W. N., & Ahrens, J. P. (1981). *Estimation of wave reflection and energy dissipation coefficients for beaches, revetments, and breakwaters* (No. CERC-TP-81-1). COASTAL ENGINEERING RESEARCH CENTER FORT BELVOIR VA.

Stelling, G., & Zijlema, M. (2003). An accurate and efficient finite-difference algorithm for non-hydrostatic free-surface flow with application to wave propagation. *International Journal for Numerical Methods in Fluids*, *43*(1), 1-23.

Symonds, G., Huntley, D. A., & Bowen, A. J. (1982). Two-dimensional surf beat: Long wave generation by a time-varying breakpoint. *Journal of Geophysical Research: Oceans (1978–2012)*, *87*(C1), 492-498.

VAN DER MOLEN, W., MONARDEZ, P. & VAN DONGEREN, A. 2006. Numerical simulation of long-period waves and ship motions in Tomakomai Port, Japan. Coastal Engineering Journal, 48, 59-79.

Zijlema, M., Stelling, G., & Smit, P. (2011). SWASH: An operational public domain code for simulating wave fields and rapidly varied flows in coastal waters. *Coastal Engineering*, *58*(10), 992-1012.

Zijlema, M., & Stelling, G. S. (2008). Efficient computation of surf zone waves using the nonlinear shallow water equations with non-hydrostatic pressure. *Coastal Engineering*, *55*(10), 780-790.

Zijlema, M., & Stelling, G. S. (2005). Further experiences with computing non-hydrostatic free-surface flows involving water waves. *International journal for numerical methods in fluids*, *48*(2), 169-197.

Appendices

A linear wave theory

In chapter 2 linear wave theory is discussed briefly, below a more detailed description is given.

The following set linearized equations and boundary conditions are to describe two-dimensional fluid motion on a horizontal bottom.

$$\frac{\partial^2 \phi}{\partial x^2} + \frac{\partial^2 \phi}{\partial z^2} = 0$$

$$\frac{\partial \phi}{\partial z} = \frac{\partial \eta}{\partial t} \quad \text{and} \quad \frac{\partial \phi}{\partial t} + g\eta = 0 \quad \text{at} \quad z = 0$$

$$\frac{\partial \phi}{\partial z} = 0 \quad \text{at} \quad z = -h$$

Where ϕ is the velocity potential, x the horizontal coordinate, z the vertical coordinate pointing up from the free surface, g the acceleration of gravity, t the time and h the water depth (for definitions see Figure 27). The above set of equation is obtained upon assuming that the amplitude a of the surface elevation η is small compared to the depth h and wavelength L. This means, the linear approximation assumes a weakly disturbed surface. Solving the Laplace equation for a sine wave propagating in positive x-direction with wave height H, period T and wavelength L,(see Figure 27), η becomes:

$$\eta(x,t) = \frac{1}{2} H \sin\left(\frac{2\pi}{T} - \frac{2\pi x}{L}\right)$$

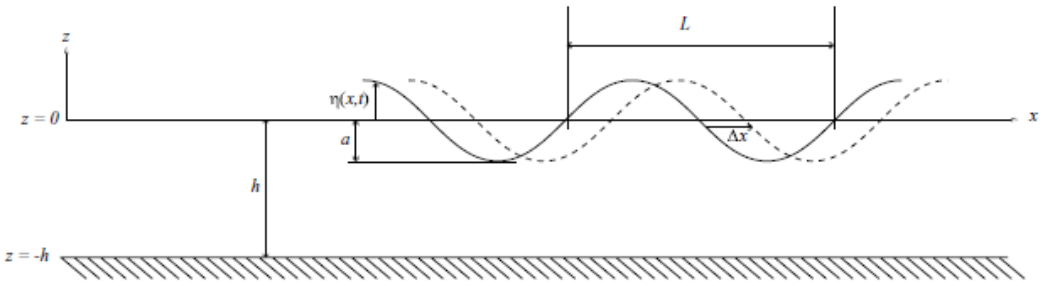

Figure 27: Directions and variables

For convenience the following parameters are defined as:

$$\text{amplitude } a = \frac{1}{2} H$$

$$\text{angular frequency } \omega = \frac{2\pi}{T}$$

$$\text{wave number } k = \frac{2\pi}{L}$$

And the surface elevation can be written as:

$$\eta(t, x) = a \sin(\omega t - kx)$$

The phase speed c of this wave can be expressed as:

$$c = \frac{\omega}{k} = \frac{L}{T}$$

Solving the Laplace equation for with above boundary conditions leads to

$$\phi(x, z, t) = \frac{wa}{k} \frac{\cosh(k(h+z))}{\sinh(kh)} \cos(wt - kx)$$

From this the linear dispersion can be determined

$$\omega^2 = gk \tanh(kh)$$

This relation between wavenumber and frequency is referred to as the linear dispersion relation for free surface gravity waves. The dispersion relation determines the speed of disturbance propagation in a certain region for a given frequency. From this an expression for the phase velocity can be derived.

$$c^2 = \frac{\omega^2}{k^2} = \frac{g}{k} \tanh kh \quad \text{or} \quad c = \sqrt{\frac{gL}{2\pi} \tanh \frac{2\pi h}{L}}$$

Using the properties of the properties of the hyperbolic functions this equation can be simplified for certain relative depth regions (expressed by the relative depth kh-factor). The wave propagation velocity c_d for relatively deep water (kh >>1), thus $\tanh(kh) \approx$ 1m, becomes then

$$c_d \approx \frac{g}{\omega}$$

In shallow water where kh <<1, thus $\tanh(kh) = kh$, k can be eliminated from the linear dispersion relationship and velocity c_s can be derived

$$c_s = \sqrt{gh}$$

Energy

The energy in a wave field consists of two parts, the kinetic energy and the potential energy. The mean kinetic energy can be expressed as

$$E_k = \frac{1}{2}\rho \overline{\int_{-h}^{\eta} |u|^2 \, dz}$$

With $u = \left[\frac{\partial \phi}{\partial x} + \frac{\partial \phi}{\partial z} \right]$ assuming the disturbance to be of small amplitude, the pervious equation can be written as:

$$E_k = \frac{1}{2}\rho \int_{-h}^{0} \overline{|u|}^2 \, dz$$

And upon substituting $\frac{\partial \phi}{\partial x}$ and $\frac{\partial \phi}{\partial z}$ this gives

$$E_k = \frac{\rho(\omega a)^2}{4k} \coth kh$$

Upon applying the linear dispersion relationship the previous equation reduces to

$$E_k = \frac{1}{4}\rho g a^2$$

In a conservative dynamic system with small oscillations the mean kinetic energy is equal to the mean potential energy. This leads to the following expression for the total mean energy per unit of surface area E_t.

$$E_t = 2E_k = \frac{1}{2}\rho g a^2$$

Energy flux

The mean rate of energy transfer F of waves parallel to the direction of propagation can be written

$$F = Enc \quad \text{with} \quad n = \frac{1}{2} + \frac{kh}{\sinh 2kh}$$

The dimensionless parameter n depends only on kh, and thus the relative depth. The velocity at which energy of a certain wave field, the wave front, propagates in an undisturbed region is expressed by

$$c_g = \frac{\partial \omega}{\partial k} = nc$$

Where c_g is called the group velocity. This implies that individual wave crests travel with a relative velocity (c - nc) with respect to the envelope see Figure 28. It follows that the group speed c_g varies between 0.5 and 1.0 times the phase speed for deep and shallow water respectively; i.e. in shallow water the group speed equals the phase speed, while in deep water the group speed equals half the phase speed.

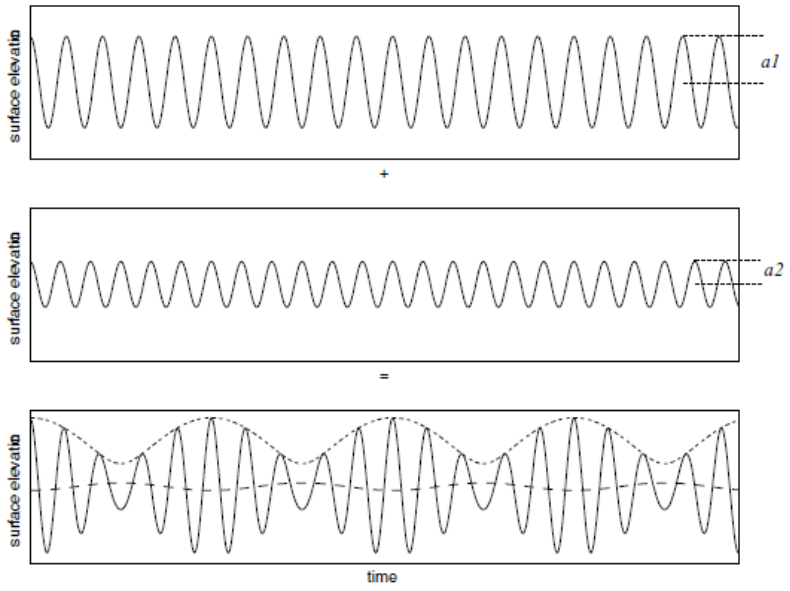

Figure 28: Upper two panels show the primary waves (solid lines), the lowest panel shows the superposition of the two primary waves and the amplitude envelope. The dash-dot line represents the bound long wave

Radiation stress

Physically, radiation stress is the excess transport of horizontal momentum due to the presence of waves. The total momentum transport through a vertical plane per unit width is water depth h and surface elevation eta consists of two parts. An advection component, which can be written

$$\int_{-h}^{\eta} \rho u^2 dz$$

And a pressure component, which can be written

$$\int_{-h}^{\eta} p dz$$

Where p represents the pressure, u the horizontal particle velocity and ρ the density of the fluid. Adding these contributions and time-averaging over an integer number of periods yields

$$\overline{\int_{-h}^{\eta} (p + \rho u^2) dz}$$

The overline denotes the time averaging operation. The excess momentum transport due to the waves is determined by subtracting the transport of momentum without waves yielding

$$S_{xx} \equiv \overline{\int_{-h}^{\eta} \left(p + \rho u^2 \right) dz} - \int_{-h}^{0} p_0 dz$$

Applying linear theory, the following expression can be found for S_{xx}

$$S_{xx} = E\left(\frac{2kh}{\sinh(2kh) + \frac{1}{2}} \right) \quad \text{or} \quad S_{xx} = E(2n - \frac{1}{2})$$

Shoaling free waves

Considering cross-shore energy flux on a sloping beach, uniform in alongshore direction, while assuming negligible dissipation, the energy flux F must remain constant; i.e F = constant in cross-shore direction. In terms of amplitude this can be written as

$$\frac{F_1}{F_2} = \frac{E_1 c_{g1}}{E_2 c_{g2}} = 1 \Rightarrow \frac{a_2}{a1} = \sqrt{\frac{c_{g1}}{c_2}}$$

Where subscripts denote a cross-shore position. For shallow water $c_g \approx \sqrt{gh}$ it can be seen that the amplitude varies proportional to $h^{1/4}$. This shoaling behaviour is referred as Green's law. With a reference point located on deep water, denoted by 0 as subscript, we can define a shoaling factor K_s

$$K_s = \sqrt{\frac{c_{g0}}{c_g}}$$

Long waves

This section focuses on low frequency (LF) waves and describes various theories concerned with the generation and releasing mechanisms of these low frequency long waves. Assume the length of a wave group long compared to the depth. This allows to depth and time average the conservation equation governing the motion of the fluid. For a one-dimensional situation (e.g. a flume) these equations for mass and momentum conservation can be written as:

$$\frac{\partial \bar{\eta}}{\partial t} + \frac{\partial}{\partial x}\left(\left(h + \bar{\eta}\right)U\right) = 0$$

$$\frac{\partial U}{\partial t} + U\frac{\partial U}{\partial x} + g\frac{\partial \bar{\eta}}{\partial x} = \frac{-1}{\rho\left(h + \bar{\eta}\right)}\frac{\partial S_{xx}}{\partial x}$$

Where $\bar{\eta}$ the surface elevation averaged over the short wave period and U is the corresponding depth averaged long wave particle velocity. The above equations are the non-linear shallow water equations with a forcing term and change into linear equations when $\bar{\eta} << h$ is assumed. In that case the linearized equations read

$$\frac{\partial \bar{\eta}}{\partial t} + \frac{\partial}{\partial x}\left(hU\right) = 0$$

$$\frac{\partial U}{\partial t} + g\frac{\partial \bar{\eta}}{\partial x} = \frac{-1}{\rho h}\frac{\partial S_{xx}}{\partial x}$$

Generation

When evaluating a situation with a horizontal bottom, the previous equation can be written as

$$\frac{\partial \bar{\eta}}{\partial t} + h\left(\frac{\partial U}{\partial x}\right) = 0$$

The amplitude modulations travel with the group velocity c_g, hence the $\frac{\partial}{\partial t}$ term can be replaced with $-c_g\frac{\partial}{\partial x}$. The following expressions can be obtained

$$-c_g \frac{\partial \bar{\eta}}{\partial x} + h \frac{\partial U}{\partial x} \quad \text{and}$$

$$-c_g \frac{\partial U}{\partial x} + h \frac{\partial \bar{\eta}}{\partial x} = \frac{-1}{\rho h} \frac{\partial S_{xx}}{\partial x}$$

Elimination of U and integrating with respect to x yield the surface elevation of the long wave motion

$$\bar{\eta} = -\frac{S_{xx}}{\rho\left(gh - c_g^2\right)} + C$$

Where integration constant C may be chosen as zero. This means that the LF surface elevation is negatively correlated with local short wave amplitude. This can be understood by considering $-\frac{\partial S_{xx}}{\partial x}$ as a pressure applied on the water. It can be seen from (2.34) that if the group speed c_g approaches the shallow water limit, $\sqrt{gh}$ the denominator approaches zero and $\bar{\eta}$ will released. Due to the breaking process the short waves will not reach the very shallow parts of a slope in practice but for shallow water $c_g^2 \approx gh\left[1-(kh)^2 + O(kh)^4\right]$ can be adopted and (2.34) can be written as

$$\bar{\eta} \approx \frac{-S_{xx}}{\rho g h (kh)^2}$$

It can be seen from (2.10) that $k^2 \approx \frac{\omega^2}{gh} O((kh)^2)$ and (2.35) changes into

$$\bar{\eta} = \frac{-S_{xx}}{\rho \omega^2 h^2} = -\frac{3ga^2}{4\omega^2 h^2}$$

B SWASH

The governing equations are the non-linear shallow water equations including the non-hydrostatic pressure. SWASH considers both the depth-averaged version of these equations as the multi-layer case, by which the vertical domain is divided in several terrain following layers. The equations implemented in SWASH are

$$\frac{\partial \xi}{\partial t}+\frac{\partial hu}{\partial x}+\frac{\partial hv}{\partial y}=0$$

$$\frac{\partial u}{\partial t}+\frac{\partial u}{\partial x}+v\frac{\partial u}{\partial y}+g\frac{\partial \xi}{\partial x}+\frac{1}{h}\int_{-d}^{\xi}\frac{\partial q}{\partial x}dz+c_f\frac{u\sqrt{u^2+v^2}}{h}=\frac{1}{h}\left(\frac{\partial h\tau_{xx}}{\partial x}+\frac{\partial h\tau_{xy}}{\partial y}\right)$$

$$\frac{\partial v}{\partial t}+u\frac{\partial u}{\partial x}+v\frac{\partial v}{\partial y}+g\frac{\partial \xi}{\partial y}+\frac{1}{h}\int_{-d}^{\xi}\frac{\partial q}{\partial x}dz+c_f\frac{u\sqrt{u^2+v^2}}{h}=\frac{1}{h}\left(\frac{\partial h\tau_{yx}}{\partial x}+\frac{\partial h\tau_{yy}}{\partial y}\right)$$

The equations are solved in time t and in horizontal directions x and y (located at the still water depth d with positive z-axis in upward direction), ξ is the surface elevation measured form the still water depth so that the total depth is given by $h=d+\xi$, u and v are the depth averaged flow velocities in x and y direction, respectively, the non-hydrostatic pressure term is given by q, c_f is the dimensionless bottom friction coefficient and τ_{ij} represent the horizontal turbulent stresses.

Porous flows

SWASH got extends into covering porous flow and the ability to predict partial reflection and transmission. The Forchheimer relation is included in the porous momentum equation by means of two extra friction terms fi and ft . Every grid cell has a porosity ranging from n=0 (wall) till n=1 (pure water). The derviation of the Forchheimer relation is give below.

Forchheimer added a quadratic term to the Darcy law and proposed the following formula:

$$I=au_f+bu_f\left|u_f\right|$$

Where I is the pressure gradient, u_f = filter velocity

There are many different formulations for the constant a and b in the Forchheimer fomula. The formulation which is directly derived from the Navier-Stokes equation is used. This derivation is described by Burcharth and Andersen (1995).

$$\frac{Du}{Dt}=-\frac{1}{\rho_w}\nabla p+\nu\nabla^2 u+G$$

Using the following assumptions on the previous equation it possibly to derive a simplification:

1. Only one dimension flow in x direction is considered
2. The hydraulic pressure gradient can be written as $I = -\frac{1}{\rho_w g}\frac{\partial p}{\partial x}$
3. Only consider pressure driven flow so the gravitational term could be written in the pressure term
4. Only consider stationary flow so $\frac{\partial u}{\partial t} = 0$

The Navier-stokes equation could then be written as:

$$I = \frac{\nu}{g}\left(\frac{\partial^2 u}{\partial x^2}\right) + \frac{u}{g}\frac{\partial u}{\partial x}$$

If u_k and D are used as characteristic speed and length parameter, and by using the non-dimensional constants α and β, the equation could then be written as:

$$I = \alpha\frac{\nu}{g}\left(\frac{u_k}{D^2}\right) + \beta\frac{1}{g}\frac{u_k}{D}$$

By substituting u_k with u_f/n, where u_f is a filter velocity and n is the porosity, and also substituting D with the hydraulic radius R (defined as the ratio of pore volume over pore surface area), this result in:

$$I = \alpha\frac{(1-n)^2}{n^3}\frac{\nu}{g{d_{n50}}^2}u_f + \beta\frac{(1-n)}{n^3}\frac{1}{g{d_{n50}}^2}{u_f}^2$$

Note that the Forchheimer coefficients a and b are now defined by a formula with a new coefficient α and β as in the previous equation. In order to solve to solve the equations, the value for α and β have to determined. These constants have to be experimentally determined and are only applicable for a certain flow regime.

C Signal decomposition

The collocated method decomposes the signal in the time domain based on both the surface elevation and velocity signal of the long waves (Guza et al., 1984).

The time series of the surface and velocity signal of linear waves unidirectional in x-direction can be written according:

$$\zeta(x,t) = \zeta^{+}(x,t) + \zeta^{-}(x,t)$$

$$u(x,t) = u^{+}(x,t) + u^{-}(x,t)$$

Where superscript + and – denote the incoming and outgoing component respectively. Considering very shallow water, the velocity is given by the next equation, with the angular frequency ω, wave period k and long waves surface elevation ζ. The ratio of the angular frequency and the wave number can be written as the phase speed of an individual wave.

$$u = \frac{\omega}{kh}\zeta = \frac{c}{h}\zeta$$

Substituting the previous equation for the incoming and outgoing long waves velocity signal results in the following equation, dropping the spatial and time dependency. The minus sign in the RHS results form the velocity of the outgoing wave which is negative due to its direction.

$$u = c^{+}\frac{\zeta^{+}}{h} - c^{-}\frac{\zeta^{-}}{h}$$

The equations for the surface elevation in the positive and negative direction form a set of equations with unknowns (ζ^{+} and ζ^{-}). Solving the set of equations for the incoming and outgoing surface elevation results in:

$$\zeta^{+} = \frac{c^{-}\zeta - uh}{c^{+} + c^{-}}$$

$$\zeta^{-} = \frac{c^{+}\zeta - uh}{c^{+} + c^{-}}$$

The incoming long waves are assumed to be found and to propagate with the group velocity corresponding to the peak period of the short wave spectrum; the outgoing long waves are free waves propagating with the phase velocity (assuming very shallow water). If the in- and outgoing waves are assumed to propagate with the very shallow water phase velocity, the solution according to Guza et al. (1984) is recovered:

$$\zeta^{+} = \frac{1}{2}\left(\zeta + \sqrt{\frac{h}{g}}\right)$$

$$\zeta^{-} = \frac{1}{2}\left(\zeta - \sqrt{\frac{h}{g}}\right)$$